AD 286 471

D1-82-0196

BOEING SCIENTIFIC RESEARCH LABORATORIES

Measurements of Lunar Temperature Variations During an Eclipse and Throughout a Lunation

Richard W. Shorthill

August 1962

Geo-Astrophysics Laboratory

D1-82-0196

MEASUREMENTS OF LUNAR TEMPERATURE VARIATIONS DURING AN ECLIPSE AND THROUGHOUT A LUNATION

by

Richard W. Shorthill
Geo-Astrophysics Laboratory
Boeing Scientific Research Laboratories
Seattle 24, Washington

A paper presented at the Conference on Lunar Exploration held at the Virginia Polytechnic Institute, Blacksburg, Virginia on August 13-17, 1962. Sponsored by VPI, NASA and NSF.

August 1962

TABLE OF CONTENTS

Introduction

Infrared Measurements: During a Lunation

Infrared Measurements: During an Eclipse

Radio Measurements: During a Lunation

Radio Measurements: During an Eclipse

Recent Measurements: Infrared

Crater Surveys

Summary of Crater Surveys:

Illuminated Moon:

Eclipsed Moon:

Review of Calculated Results

References

Figures

ERRATUM

Fig. 7

Now reads: 0.92 Illuminated (~ 18 Day Old Moon)

Should read: 0.96 Illuminated (~ 17 Day Old Moon)

LIST OF FIGURES

Fig. 1 Temperature Variation During a Lunation

Fig. 2 Distribution of Planetary Heat Across the Disk of the Full Moon After Pettit and Nicholson

Fig. 3 Roughness Factor Explanation of $\cos^{2/3} \theta$ Variation in Observed Energy Over Lunar Disk at Full Moon

Fig. 4 Isothermal Contours of May 16, 1959 Start 1:49, End 4:43 UT, 58 Scans 0.53 Illuminated (~ 8 Day Old Moon)

Fig. 5 Isothermal Contours of November 10, 1959 Start 2:17, End 5:23 UT, 63 Scans 0.77 Illuminated (~ 10 Day Old Moon) Plotted on a Simultaneous Photograph

Fig. 6 Isothermal Contours of September 26, 1958, Start 3:55, End 7:01 UT, 63 Scans 0.98 Illuminated (~ 14 Day Old Moon)

Fig. 7 Isothermal Contours of March 26, 1959, Start 7:40, End 10:58 UT, 66 Scans, 0.96 Illuminated (~ 17 Day Old Moon)

Fig. 8 Isothermal Contours of January 27, 1959, Start 7:42, End 10:39 UT, 60 Scans, 0.92 Illuminated (~ 18 Day Old Moon)

Fig. 9 Roughness Factor Explanation of Decrease in Observed Subsolar Energy for Phase Angles Other Than at Full Moon

Fig. 10 Eclipse Cooling Curves for One Point 1927 and 1939 After Pettit and Nicholson

Fig. 11 Result of Gibson's Radio Measurements at 8.6 mm for Center of Lunar Disk

Fig. 12 Gibson's Observed Temperatures During Total Eclipse at 8.6 mm (Altitude 17° at Start)

Fig. 13 Brightness Contours at 4.3 mm Wavelength 77° Lunar Phase

Fig. 14 Brightness Contours at 4.3 mm Wavelength 126° Lunar Phase

Fig. 15 Brightness Contours at 4.3 mm Wavelength 280° Lunar Phase

Fig. 16 Eclipsed Moon September 5, 1960 (During Totality)

Fig. 17 The 73-Inch Reflecting Telescope of the Dominion Astrophysical Observatory, Victoria B. C. The Detector Subtended 7" of Arc at the f/5 Newtonian Focus

Fig. 18 Scanning Cycle March 12, 1960 a. Aristarchus b. End of Scan Off East Limb c. End of Scan Near the Sea of Nectar d. Center of Disk, End of 14.5 Min. Scan Cycle e. Copernicus

Fig. 19 Scan Over the Lunar Surface with Rotating Filter Wheel During the Full Moon March 12, 1960 (The Open Filter Shows Radiation from 0.5 to 15 Microns. The Microscope Cover Glass Shows the Radiation 0.5 to 5 Microns. The Germanium Filter Shows the Radiation 2 to 15 Microns.)

Fig. 20 Original and Smoothed Data from a Typical Scan of the Crater Tycho March 12, 1960

Fig. 21 Scan Path Over Tycho September 5, 1960

Fig. 22 Simulated Atmospheric Transmission Curve

Fig. 23 Calibration Curves From Sky and Subsolar Point Readings

Fig. 24 Crater Region Scanned, September 4, 5, 6 1960

Fig. 25 Region of Aristarchus

Fig. 26 Isotherms in the Region of Aristarchus September 6, 1960 6:56 UT

Fig. 27 Isotherms in the Region of Aristarchus September 5, 1960 6:57 UT

Fig. 28 Isotherms in the Region of Aristarchus Rectified to Remove the Effect of the Curvature of the Surface September 5, 1960, 6:57 UT

Fig. 29 Isotherms in the Region of Copernicus September 6, 1960, 6:27 UT

Fig. 30 Isotherms in the Region of Copernicus September 5, 1960, 5:48 UT

Fig. 31 Isotherms in the Region of Menelaus September 5, 1960, 7:44 UT

Fig. 32 Isotherms in the Region of Tycho September 5, 1960, 5:18 UT

Fig. 33 Isotherms in the Region of Tycho September 6, 1960, 5:50 UT

Fig. 34 Isotherms in the Region of Proclus September 6, 1960, 7:54 UT

Fig. 35 Isotherms in the Region of Alphonsus September 5, 1960, 6:18 UT

Fig. 36 Temperature Traces Over Aristarchus During Eclipse, September 5, 1960

Fig. 37 Eclipse Cooling Curve for the Crater Aristarchus and its Environs

Fig. 38 Difference in Energy Ratios Between Crater and Interpolated Environs for Aristarchus September 5, 1960, Eclipse

Fig. 39 Isotherms in the Region of Aristarchus During Eclipse September 5, 1960, 10:12 UT

Fig. 40 Isotherms in the Region of Tycho During Eclipse September 5, 1960, 10:34 UT

Fig. 41 Normalized Cooling Curves for Aristarchus and its Environs; Experimental Values and Theoretical Homogeneous Surface with Different $(K\rho c)^{-1/2}$ Values

Fig. 42 Normalized Cooling Curves for Aristarchus and its Environs; Experimental Values and Theoretical Two-Layer Model

Introduction

Most of what we know about the moon comes from observations of its radiation either by reflection or by a process of absorption and re-radiation. Lunar thermal radiation falls into the latter classification and can be detected in the far infrared and at certain radio wave lengths.

The first lunar infrared temperature measurements were made by Lord Rosse in 1868. [1] The method consisted of measuring the total radiation from the lunar disk with a thermopile, using a glass plate to separate planetary heat. This work was followed by S. P. Langley [2] and others. [3] The surface temperature was estimated to be about that of boiling water. Some, however, held that the surface temperature was very low.

The first eclipse temperature measurements were made in 1884. [4] Pettit and Nicholson [5] in 1927 made the first reliable measurements of surface temperatures both on the illuminated moon and during a total lunar eclipse. Their results have been reviewed in several books. [6, 7]

Infrared Measurements: During a Lunation

The variation of temperature for a point near the center of the lunar disk is shown in Fig. 1.* This curve is for a $(K\rho c)^{-1/2} = 435$ and a subsolar temperature of 389°K. [8] The open circles are from Sinton's measurements and the other points are from Shorthill and Saari. [9] These latter points have been adjusted to the 389°K subsolar

*All Fig. will be at the end of text. References will appear as superscripts.

point temperature and for the roughness factor. These points were measured at full moon; however, they were shifted an amount in phase angle determined by the angle of illumination and position relative to the center of the disk at the time their temperatures were measured. Sinton found that the temperature of the subsolar point at full moon was 389°K for a mean spherically emitting surface at 1.000 AU. [10] The temperature of the antisolar point was measured to be 122°K ± 5° [5] and 120°K ± 3°. [8]

Distribution of planetary heat across the disk of the full moon is shown in Fig. 2. [5] Theory would predict an energy variation according to

$$E = A \cos \theta$$

where θ = angular distance from the subsolar point and A the radius of the moon for this plot. The observed radiation, however, follows more closely

$$E = A \cos^{2/3} \theta$$

which has been accounted for by the roughness of the lunar surface. As one moves away from the center of the lunar disk the actual surface temperature decreases as $\cos^{1/4} \theta$, but this variation as seen from the earth is altered by the fact that only illuminated surfaces are seen at full moon. The valleys, slopes and peaks are illuminated near the center of the disk while the valleys on the limb (Fig. 3) are not completely illuminated and therefore a higher temperature is observed. $T_{observed} = T_{ssp} \cos^{1/6} \theta$ applies to the observed full moon temperatures.

Some published results of Sinton [10] are shown in Fig. 4. A Golay cell was used to make these series of temperature surveys. The moon was scanned like a TV picture at the rate of three minutes per single scan. The resolution was 25" of arc (47 km at center of disk). Fig. 5 [10] shows an overlay for about a ten day old moon. The subsolar point is indicated by (+) sign. At this phase the observed subsolar point temperature is $373^{\circ} < T_{ssp} < 383^{\circ}K$. It is noted that Mare Crisium seems to appear as a warmer region. Sinton has related the thermal contours to general features. The south-polar regions appear somewhat cooler than the north-polar regions. North is at the top as in Fig. 6 [10] for about a fourteen day old moon. The right ascension and declination axes are shown by the ($^{N}\times$) sign. In Fig. 7 [10] the isothermal contours over the seventeen day old moon are seen. The ($\dagger$) sign is used to indicate the origin of the selenographic coordinate system. Horizontal structure or abnormal excursions parallel to the right ascension motion are seen in all these contours. (This noise may be caused by sudden shifts in the sky background radiation or scanning errors). Fig. 8 [10] shows another isothermal contour over the entire disk of the moon with 25" of arc resolution indicated by the circle labled 3mm.

The decrease of the observed subsolar point temperature at large phase angles is a result of the surface roughness. Valleys should be warmer since they receive radiation from more than a hemisphere. A lower temperature is observed because these valleys are not seen at large lunar phase angles. Fig. 9 illustrates this

effect of roughness.

Infrared Measurements: During an Eclipse

In 1927 Pettit and Nicholson measured the temperature variation in the 10-14 micron band at a point near the southern limb. Pettit in 1939 measured a point near the center of the lunar disk. Their results are shown in Fig. 10. Strong and Sinton [11] observed an eclipse in 1953. They found that the limb areas, cooler to start with, lost a larger fraction of their heat. They explained this in terms of surface roughness. The depressions on the limb areas are not observed, they cool less rapidly because they cannot radiate to a full hemisphere. The cooling of the limb peaks is observed and since they can radiate more nearly to a hemisphere an apparent larger fraction of heat loss is noted.

Radio Measurements: During a Lunation

It is not intended to give a complete review of radio thermal emission but only an indication of some of the results. See reference 6 and reference 8 for a more complete review. When lunar thermal radiation is measured at relatively short wave lengths two features are noticed. First, the average temperature is lower than that measured in the 8 to 14 micron band and second, there is a phase lag relative to the optical phase of the moon. Gibson's measurements were made at the 8.6mm wave length [12] during a lunation and an eclipse. The results are shown in Fig. 11 and Fig. 12. This radiation comes from below the lunar surface, that is, the lunar surface is somewhat transparent at these wave lengths. As the probing wave length increases

the depth of the layers contributing to this radiation therefore increases. The problem is further complicated by the fact that all the upper layers contribute to the observed temperatures as well. Another very interesting set of contour maps was made by R. J. Coates. [13] They are included here as an example of how radio temperature measurements may be correlated with visible features. These were made at 4.3mm with 6.'7 of arc resolution (~ 1/5 lunar diameter). The brightness temperature for the center of the disk (Fig. 13) as given by the author is 182°K. This map was made near first quarter. The contours over Tranquillitatis, Foecunditatis and Nectaris follow the general shape of this region. These regions seem to heat up more rapidly than the surrounding mountain areas. It is also noticed that Procellarum is slightly brighter than the surrounding mountains. At 126° lunar phase (Fig. 14) the brightness temperature of the center of the disk is now 243°K. Maria Tranquillitatis, Foecunditatis and Nectaris are now more uniformly bright. Mare Imbrium, however, remained cooler - just opposite the effect of the other maria with the same illumination. At third quarter (Fig. 15) the brightness temperature of the center of the disk is 254°K. Mare Tranquillitatis is now cooler than the surrounding mountains. Maria Nubium and Humorum follow the brightness contours. Imbrium is now cooler than its surroundings. Coates concludes by stating that at 4.3mm the maria heat up more rapidly and cool off more rapidly than the mountain regions. Imbrium is an exception and remains cooler throughout the lunar cycle. Since

the characteristics of the moon at millimeter wave lengths are not the same for all regions it would be useful to repeat certain longer wave length measurements with higher resolution in order to study these characteristics.

Measurements have been made at radio wave lengths from 0.15cm to 168cm. [14] Variations with lunar phase have been detected at the shorter wave lengths with a lag as much as 50° lunar phase angle. At the longer wave lengths little or no variation is found. Also at the longer wave lengths only the average disk temperature is measured and is averaged over a certain depth as well.

Radio Measurements: During an Eclipse

Eclipse measurements at 8.6mm were shown in Fig. 12. At this wave length no variation was observed. Sinton [15] did report a variation at 1.5mm wave length with about an hour phase lag. Later measurements did not show any variation; however, conditions were not the most favorable for observations.

Recent Measurements: Infrared

An eclipse of the moon is exciting to observe both visually and with a radiometer - if you choose the proper wave length! Fig. 16 is a reproduction of a color negative taken during totality of the lunar eclipse of September 5, 1960. In an attempt to detect variations from the previously described cooling characteristics Shorthill, Borough and Conley [16] measured the infrared lunar thermal radiation with improved spatial resolution. With a Barnes' thermistor bolometer mounted at the Newtonian focus (Fig. 17) the lunar surface was scanned

with 7" of arc resolution (12 km at center of disk). The KRS-5 window limited the spectral bandpass to the 0.5-40 micron band. A germanium filter was used to further limit the bandpass to the infrared region. The rms noise level corresponded to a radiation flux of 3×10^{-9} watts for a 10 cps bandwidth. The radiation was mechanical chopped at 80 cps and synchronously rectified. The scanning cycle is shown in Fig. 18 which was designed to include many different types of regions such as mountains, bright and rayed areas and features reported to have shown activity of some kind. Fig. 19 shows an example of one scan path. A filter wheel with six positions rotated in front of the KRS-5 window. Three positions were open filter (no filter), two positions were microscope cover glass and one position was germanium filter. Note that in several areas the reflected light, passed by the microscope cover glass decreases, while the infrared deflection, passed by the germanium filter, remains at the same level. Clouds prevented the carrying out of the complete scanning program during the penumbral phase. During the umbral phase however, the seeing was good and the sky background produced a constant deflection. The lunar surface was now somewhat below 200°K. It was discovered that Aristarchus and Copernicus produced deflections greater than the general lunar background. No other deflections were noted in the area covered by the scanning cycle. The crater Alphonsus was scanned several times and no deflections above its' environs were observed.

When the crater Tycho was scanned a deflection above the local background by at least a factor of two was observed. The actual chart recording is shown in Fig. 20. The scan rate for Tycho was 30" of arc per minute of time. On each trace a sharp rise occurred near the south rim, gradually decreasing toward the north rim; however, due to collimation uncertainty the rise could not be definitely ascribed to the rim of the crater. Tycho is about 40° above its environs.

The three lunar features found to exhibit this enhanced radiation during an eclipse were all rayed craters. The most immediate interpretation of these observations was that the rayed craters are covered by a thinner dust layer. Other interpretations are open, such as vulcanism, radioactivity and emissivity variations. Further, the data do not disagree with the assumption that these craters are among the younger features on the moon.

The eclipse of September 5, 1960 provided an opportunity to make another series of measurements to verify this anomalous cooling and map the extent of this effect both spatially and in time. The instrumentation was the same except the signal was converted to FM (1.2 ± 0.5 kc) and recorded on magnetic tape. Since this was recorded with a short time constant the signal could be demodulated, smoothed with different filters and expanded or compressed in time at the laboratory to obtain optimum reduction of the data.

With the telescope drive near lunar rate the slow setting motion was used to drive east and west at about 6" of arc per second of time over the lunar surface. Combined with the normal drift in

declination a sawtooth like scan path was traced over a localized region, as shown in Fig. 21 for Tycho. Corrections were made for parallax and refraction for each scan in order to calculate the motion of the detector relative to the lunar disk.

Since we were primarily concerned with relative temperatures it was felt sufficient to calibrate on the subsolar point and the sky periodically. For the purposes of our calculations it was assumed that the subsolar point temperature was 374°K. The atmospheric transmission curve used in our calculations is shown in Fig. 22. Using the black body curve for a given temperature T_i the amount of energy $E(T_i)$ getting through the atmospheric window was determined. The ratios $E(T_i)/E(T_{374}) = R_i$ were formed. It was found that the equation

$$\log_{10} R_i = A - B/T_i + C/T_i^2$$

represented the relationship between R_i and T_i. Fig. 23 shows the calibration data from the sky and the subsolar point for one night. The energy ratios were formed such as

$$R_{moon} = \frac{E(T_{moon}) - E(T_{sky})}{E(T_{ssp}) - E(T_{sky})}$$

for each datum reading. Then R_{moon} was related to the corresponding R_i and the observed lunar surface temperature T_{moon} was found.

The error due to detector noise alone is very small, 0.25° at 374°K increasing to 2.1° at 200°K. Errors due to sky background fluctuations were measured to be higher in some cases; however, they were less than a degree at the higher temperatures, increasing toward the lower temperatures.

Crater Surveys*

About thirty isothermal maps of eleven crater regions were constructed for September 4, 5 and 6, 1960 including some during the totality of the lunar eclipse. All the original maps were made to the scale of Kuiper's Photographic Lunar Atlas. Fig. 24 shows the regions that have been mapped. The most important results are related to the prominent rayed craters Tycho, Aristarchus, Copernicus, Proclus and Kepler. The region of Aristarchus has some interesting features associated with it. In Fig. 25 the region [17] is seen in the afternoon. Herodotus, an older crater, is to the southeast, and Schröter's Valley is to the northeast. Notice the white area near the apparent end of Schröter's Valley.

Isotherms in the region of Aristarchus September 6, 1960, one day after full moon are represented in Fig. 26. This scan covered 100" of arc right ascension and 80" of arc declination. The scale is represented by the 50" of arc on the overlay. Sensor size is represented as a circle on each thermal map and amounts to 8" of arc. The hachures indicate cooler regions. Recall that this scan was made one day after full moon; the sun is still rising. The actual photograph however represents the area in the afternoon and

---

*These measurements were made on the 60-inch telescope at the Mt. Wilson Observatory in California.

the shadow configuration is not correct for the time when the scan was made. Several things are noticed:

1) The contours are related to the feature Aristarchus.
2) The crater is cooler than its general surroundings.
3) Herodotus does not seem to affect the shape of the contours directly nor does Schröter's Valley.
4) There is a general gradient in the direction of the subsolar point. This last characteristic was to be expected.

Other important features can be seen. The cooler region not only is centered on the crater but extends beyond and somewhat into Herodotus. There is a correlation with the general white area near the end of Schröter's Valley. In general the contours seem affected by the brighter areas! It is known that Aristarchus has a high albedo. Therefore it is reasonable then that more of the sun's incident radiation would be reflected, less absorbed and less re-radiated as planetary heat accounting for this lower temperature. The effect of geometry may also alter the distribution of temperature in and around a crater. This is due to the elevation angle of the sun with respect to the local surface and should change during the three day observation period. The same region about twenty-four hours before shows a 2° difference between the crater and its environs (Fig. 27). There is considerable noise or horizontal structure in the direction of scan (right ascension). If the gradient in the direction of the subsolar point (due to curvature of the lunar surface) were removed

the local character of the thermal contours can be observed. In Fig. 28 this has been accomplished, leaving the temperature of the crater center the same. As a by-product of this method some of the horizontal structure has also been removed.

Copernicus is another rayed crater over which thermal mapping was performed. The sensor diameter was between 1/5 and 1/6 crater diameters. The effect of albedo is observed here (Fig. 29), that is, the whole area in and around Copernicus is cooler than its surroundings, corresponding to the bright area around the crater. The center of the crater is 369°K and the western interior is cooler by 2.5°. The only other correlation that can be seen is the sharp gradient outside the west rim into the darker area. The night before during full moon (Fig. 30) the effect of geometry is seen in this large scan (200" of arc RA by 225" of arc declination). The observed temperature differential between the east and west interior slopes is 4° to 5°. Note again the general gradient toward the subsolar point, 358°K near Mayer to 370°K southwest of Copernicus. If the crater were not present the contours would be more parallel to each other such as the 368°K and 367°K southwest of Copernicus. The elevation angle of the sun is less for the interior southwest slope than for the interior northeast slope. The opposite is true for the exterior slopes. This gives rise to the difference in the observed temperatures and will be called the "geometry effect." It must be mentioned that variations in local albedo are superimposed and the two effects cannot be completely separated.

The effect of geometry is not apparent in the thermal map over the region of Menelaus (Fig. 31) at full moon. The crater is more uniformly illuminated and the shape of the contours around the crater reflect the effect of albedo. The cool region centered on the crater extends well beyond and follows somewhat the bright environs. The interior is perhaps cooler by 4° to 5°. There is some horizontal structure in evidence as well as an overall upward shift in temperature above the assumed subsolar point temperature. This shift is caused by an increase in sky background radiation which was not taken into account because the sky was monitored when the background was normal some time before and after this scan.

In the next two figures the region of Tycho is seen on the nights September 5 and 6, 1960 (Fig. 32 and 33). The direction of the gradient which is to the northwest on September 5 shifts to north on the 6th consistent with the motion of the subsolar point. The cooler and warmer regions in the crater move counter-clock-wise. In the larger scan on September 5 the contours follow the general outline of several other craters, Pictet, Street and Longomontanus.

One of the more complicated contours is that of the region around Proclus (Fig. 34). The gradient between Paulus Somnii and Proclus drops 6° in 16" of arc. Proclus is not much greater than the sensor size, however, due to many overlapping scans, detail in the crater can be obtained. The effect of geometry is indicated by

the cooler interior slope nearest the subsolar point. There is also a cool region around Promontorium Olivium. The last example of contours on the illuminated moon is that over Alphonsus (Fig. 35). The general effect of geometry causes the northern interior to be cooler, less than 367°K while the outside northern slopes are 369°K.

The most exciting results were obtained during the penumbral and umbral phases of the total lunar eclipse of September 5, 1960. The circumstances were as follows:

Entered penumbra	8:37 UT
Entered Umbra	9:36
Totality started	10:38
Totality ended	12:06
Left umbra	13:08
Left penumbra	14:07

Fig. 36 represents temperature traces over Aristarchus during the penumbral and part of the umbral phases. These traces were obtained by centering first on the feature moving off in right ascension for a few seconds of time then reversing in right ascension and scanning back through and well beyond the feature. The small dashed lines below the crater deflections show one of the means by which the so called interpolated environs were found. The chart deflection is proportional to $E(T_{moon}) + E(T_{sky})$ and has not been reduced to the calculated temperature values. Aristarchus entered penumbra at 8:51 UT and entered umbra at 9:56 UT. Several things are noticed:

1) The crater, cooler during the full moon, is warmer than its environs during the umbral phase.

2) The warmest point is centered on the crater and the anomaly extends beyond the crater.

3) The gradient toward the subsolar point grows less during the penumbral and into the umbral phase as expected.

Similar results were obtained on Copernicus and Kepler. Sinton also obtained comparable results for Tycho.[18] The eclipse cooling curve for the crater Aristarchus and its environs is shown in Fig. 37. The cooling curve of a point 166" of arc west of Aristarchus is almost parallel to the environ cooling curve and serves as a rough check on the method of interpolation.

In Fig. 38 the difference $R_{Crater} - R_{Environ} = \Delta R$ is shown. This parameter ΔR has been plotted because the effect of sky background is reduced. In this graph observe the following:

1) The cross over point where the temperatures of the crater and the environs are equal is $t/t_o \sim 0.2$.

2) A constant ΔR is reached at $t/t_o \sim 0.8$.

3) ΔR before eclipse is -0.044 and during totality 0.048. That is, the absolute value of the energy difference between the crater and its environs is almost constant before eclipse and during totality. This effect will require investigation during some future eclipse.

One of the so called "hot spots" [19] is shown in Fig. 39, temperature contours over Aristarchus during the eclipse. The crater is 228°K,

the environs 203°, giving a ΔT of 25°. Little is left of the gradient toward the subsolar point. The "hot spot" is centered on the crater and extends beyond as already described. There is no correlation with other features such as Herodotus or Schröter's Valley. There does, however, seem to be a significant relationship with the optically bright regions around Aristarchus shown as an unlabeled dashed line.

Hottest of the "hot spots" is the crater Tycho (Fig. 40) with an observed temperature difference of 31°. It is again maximum at the crater center falling to the background level somewhat beyond the crater. Correlations with other features are left to the reader's imagination!

The normalized cooling curves (Fig. 41) for Aristarchus and its environs are plotted with the theoretical homogeneous surface model of Jaeger.[20] The values of $(K\rho c)^{-1/2}$ depend on the initial value of temperature T_o and the duration of the penumbra t_o. The parameter $(K\rho c)^{-1/2}$ describes the family of cooling curves. Here K is thermal conductivity, ρ is the density and c is the specific heat. For terrestrial rock $(K\rho c)^{-1/2}$ is 20, for gravel or pumice it is 100, and for fine dust under the lunar environment it may be 1000. The data for the area 166" of arc west of Anstarchus fall on the interpolated environ curve in this normalized plot. This theoretical homogeneous model does not fit the experimental results from this eclipse cooling data.

If the cooling data are plotted along with the two layer model of Jaeger and Harper [21] there is better agreement between the theory

and experiment. This two layer model has a constraint determined by microwave results which is $d = 610\ K\ (K'\ \rho'\ c')^{-1/2}$ where d is the surface thickness in cm, $K = 2.8 \times 10^{-6}$ cal $cm^{-1} sec^{-1} deg^{-1}$, and $(K'\ \rho'\ c')^{-1/2}$ represents the substratum the values of which are shown on Fig. 42.

Summary of Crater Surveys:

Illuminated Moon:

1) Geometry effect - the crater interior slopes nearest the subsolar point are cooler than the interior slope farthest away. This effect is caused by the variation in inclination of the local surface.

2) Albedo effect - the bright rayed craters are cooler than their environs. In most cases the cooler area is centered on the feature and the temperature increases as one moves away from the center to the environ temperature somewhat beyond the crater. This effect is a result of the variation in local albedo. The higher the albedo the greater is the amount of the incident sunlight that is reflected resulting in a corresponding decrease in planetary heat.

3) Variation in the albedo effect for the three day period was noticed and may be related to directional effects. Many other details must be traced through a lunation before the contours around full moon can be completely explained.

Eclipsed Moon:

1) "Hot Spots" - the bright rayed craters cool less rapidly than their environs during penumbral phase. The crater is warmer than its environs during the umbral phase.

2) Extent of warm area - the warm area is centered on the crater and extends beyond in some cases, decreasing to the environ level there.

3) Only the five rayed craters observed were found to exhibit this effect. Many other features should be surveyed during another eclipse. Measurement during the lunar night may provide similar data.

4) These results could be explained as a variation in dust thickness. This interpretation will be published later.[22] Other interpretations are possible such as permeability to infrared emission, suggested by Buettner.[23]

Review of Calculated Results

Energy Ratio

Crater	Tycho	Aristarchus	Copernicus	Proclus	Kepler
$R_{initial}$	0.751	0.751	0.862	0.924	0.842
$R_{eclipse}$	0.116	0.079	0.072	0.066	0.037
Environs					
$R_{initial}$	0.771	0.791	0.905	0.936	0.842
$R_{eclipse}$	0.049	0.037	0.046	0.046	0.027

Temperature ^{o}K

Crater	Tycho	Aristarchus	Copernicus	Proclus	Kepler
$T_{initial}$	350	350	361	367	359
T_{final}	243	228	225	222	203
Environs					
$T_{initial}$	352	354	365	368	359
T_{final}	212	203	210	210	194
ΔT_{final} (Crater-Environ)	31	25	15	12	9

REFERENCES

1. Rosse, Lord, Proc. Roy. Soc. 17, 436 (1869). See also, Proc. Roy. Soc. 163, 587 (1873).

2. Langley, S. P. Mem. Nat. Acad. Sci. 4, 107 (1887).

3. Very, F. W., Astroph. J. 8, 199 (1898).
Coblentz, W. W. Phys. Rev. (Ser. 1) 24, 307 (1907).

4. Boeddicker, O. Nat. 30, 589 (1884).

5. Pettit, E. and Nicholson, S. P., Astroph. J. 71, 102 (1930).

6. Markov, A. V. (ed), The Moon - A Russian View (University of Chicago Press, Chicago, 1960).

7. Gilbert, F., Structure of the Moon's Surface (Pergamon Press, New York, 1961).

8. Sinton, W. M., Physics and Astronomy of the Moon ed. Z. Kopal (Academic Press, New York 1962) p. 407.

9. Shorthill, R. W. and Saari, J. M., "Lunar Infrared Temperature Measurements During September 4, 5 and 6, 1960" Boeing Company Document D7-2550-1, January 30, 1961.

10. Geoffrion, Ann R., Korner, Marjorie, and Sinton, W. M., Lowell Observatory Bulletin No. 106, 5 No. 1, 1 (1960).

11. Sinton, W. M., Planets and Satellites, ed. G. P. Kuiper (University of Chicago Press, Chicago, 1961) p. 438.

12. Gibson, J. E. Proc. Inst. Radio Engrs. 46, 280 (1958).

13. Coats, R. J. Astroph. J. 133, 723 (1961).

14. Baldwin, J. E., Monthly Nat. Roy. Astron. Soc. 122, 513 (1961).

15. Sinton, W. M., Astroph. J. 123, 325 (1956).

16. Shorthill, R. W., Conley, J. M. and Borough, H. C., Pub. Astron. Soc. Pac. 72, No. 429, 481 (1960).

17. Kuiper, C. P. (ed), Photographic Lunar Atlas, (University of Chicago Press, Chicago 1960).

18. Sinton, W. M., Lowell Observatory Bulletin No. 108, 5, No. 3 (1960).

19. Saari, J. M. and Shorthill, R. W., Sky and Telescopes, 21, No. 2, 80 (1961).

20. Jaeger, J. C., Australian J. Phys. 6, 10 (1953).

21. Jaeger, J. C. and Harper, A. F. A., Nature 166, 1026 (1950).

22. Saari, J. M. and Shorthill, R. W. "Infrared Mapping of Lunar Crater During the Full Moon and Total Eclipse of September 5, 1960" Boeing Document D1-82-0176, July 1962.

23. Buettner, K. J. K., Rand Report RM 3263-JPL, August 1962.

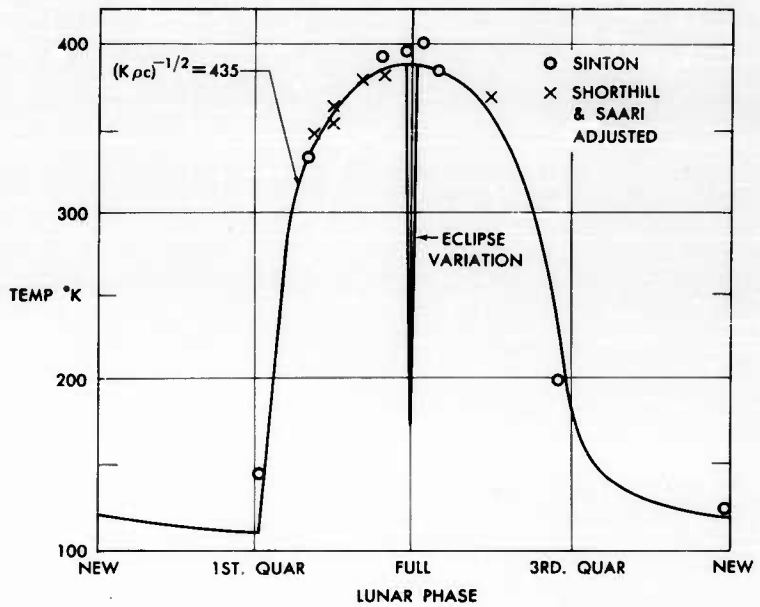

Fig. 1 Tempature Variation During a Lunation

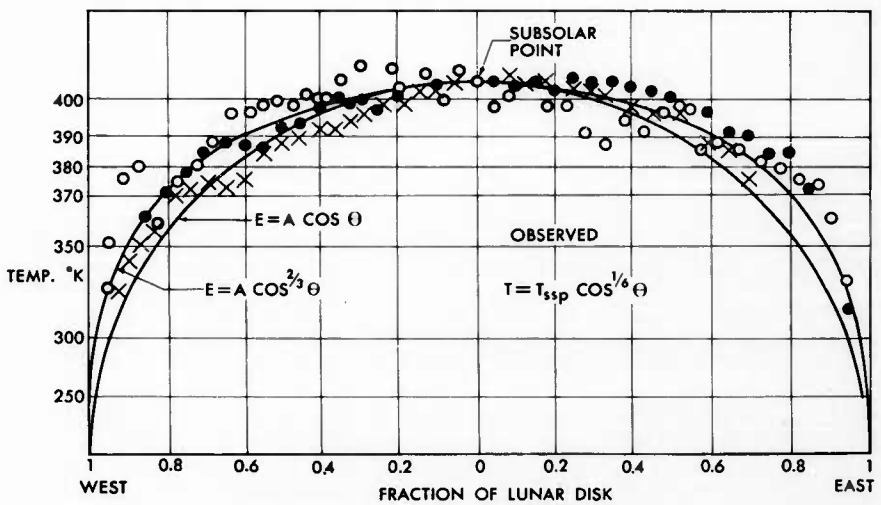

Fig. 2 Distribution of Planetary Heat Across the After Pettit and Nicholson Disk of the Full Moon

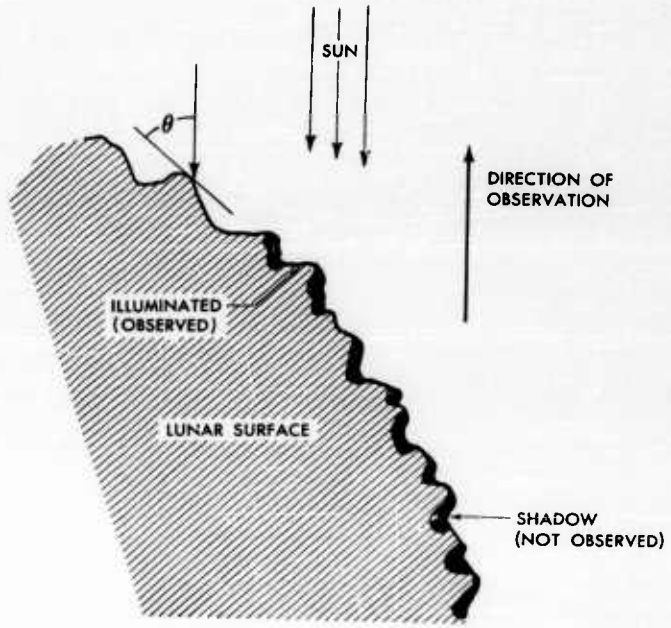

Fig. 3 Roughness Factor Explanation of Cos $^{2/3}\theta$ Variation in Observed Energy Over Lunar Disk at Full Moon

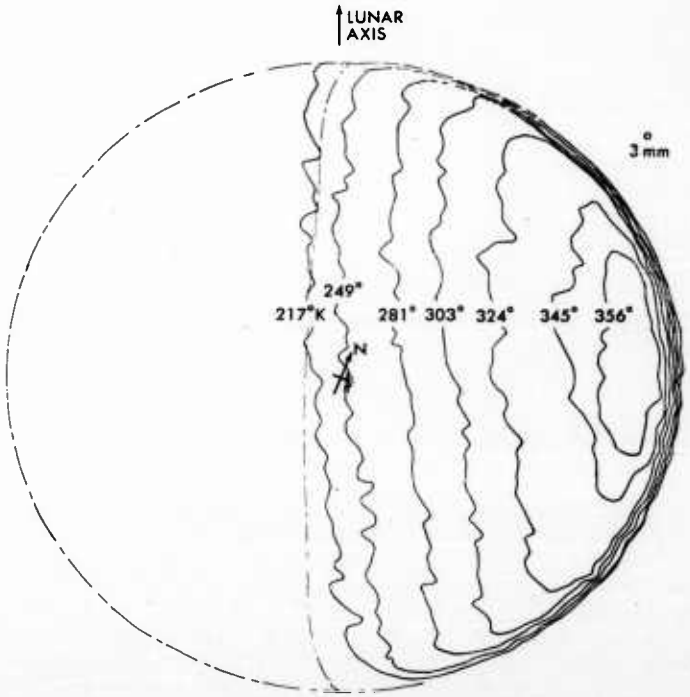

Fig. 4 Isothermal Contours of May 16, 1959 Start 1:49, End 4:43 UT, 58 Scans 0.53 Illuminated (—8 Day Old Moon)

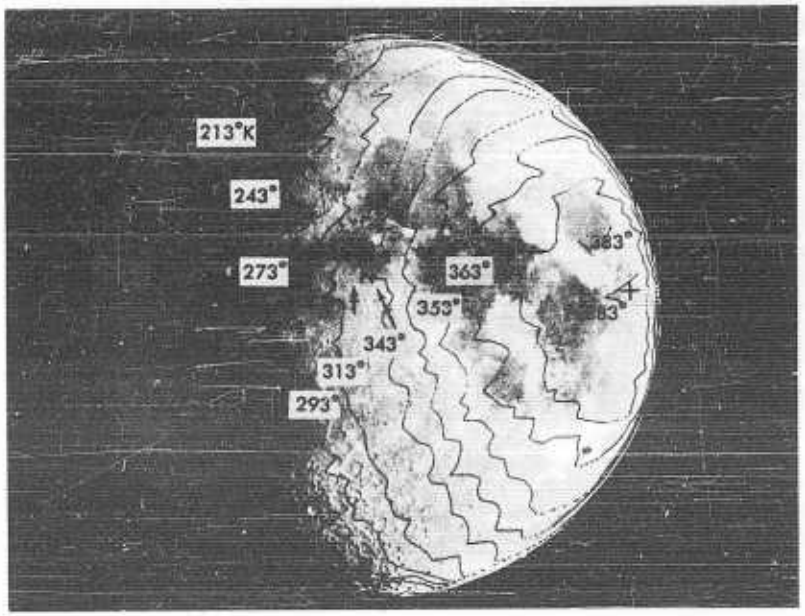

Fig. 5 Isothermal Contours of November 10, 1959 Start 2:17, End 5:23 UT, 63 Scans 0.77 Illuminated (~10 Day Old Moon) Plotted on a Simultaneous Photograph

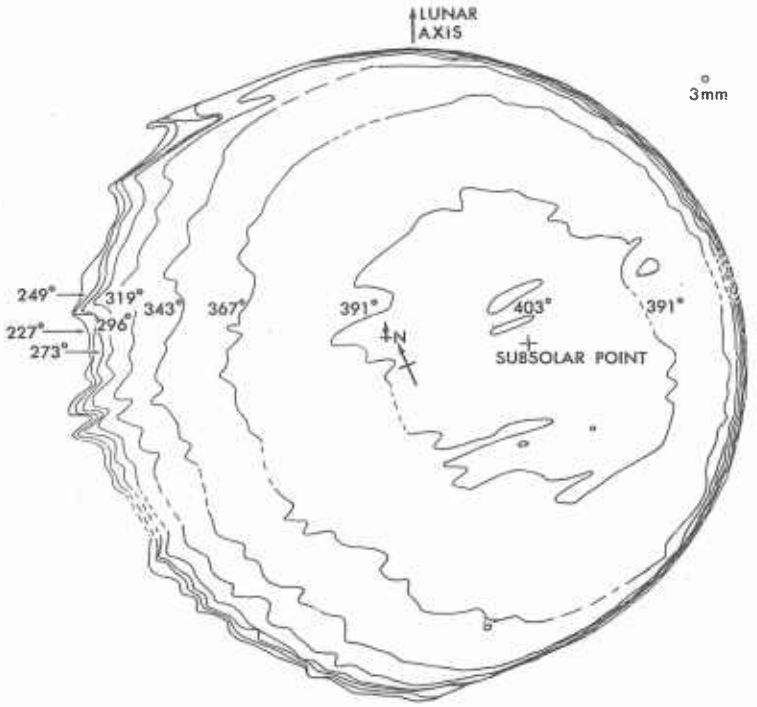

Fig. 6 Isothermal Contours of Setember 26, 1958, Start 3:55, End 7:01 UT, 63 Scans 0.98 Illuminated (~ 14 Day Old Moon)

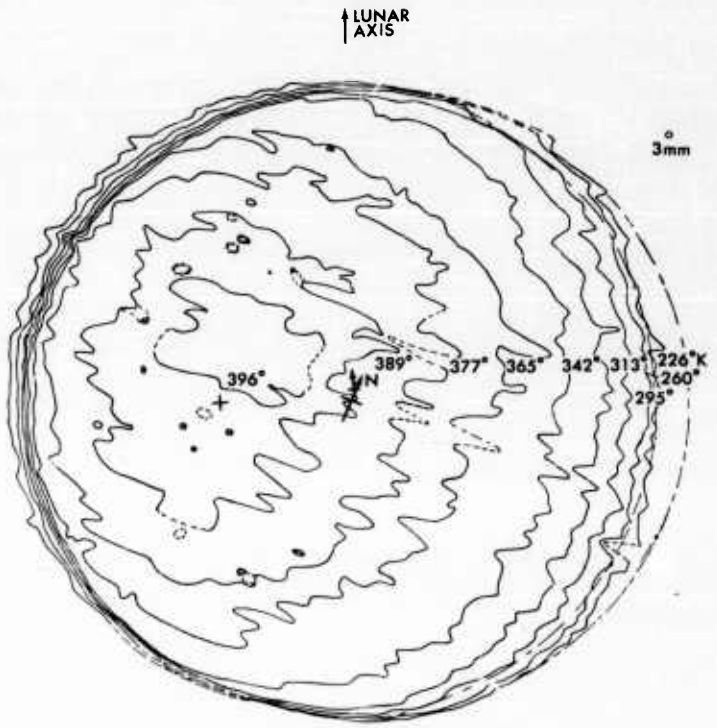

Fig. 7 Isothermal Contours of March 26, 1959, Start 7:40, End 10:58 UT, 66 Scans, 0.92 Illuminated (—18 Day Old Moon)

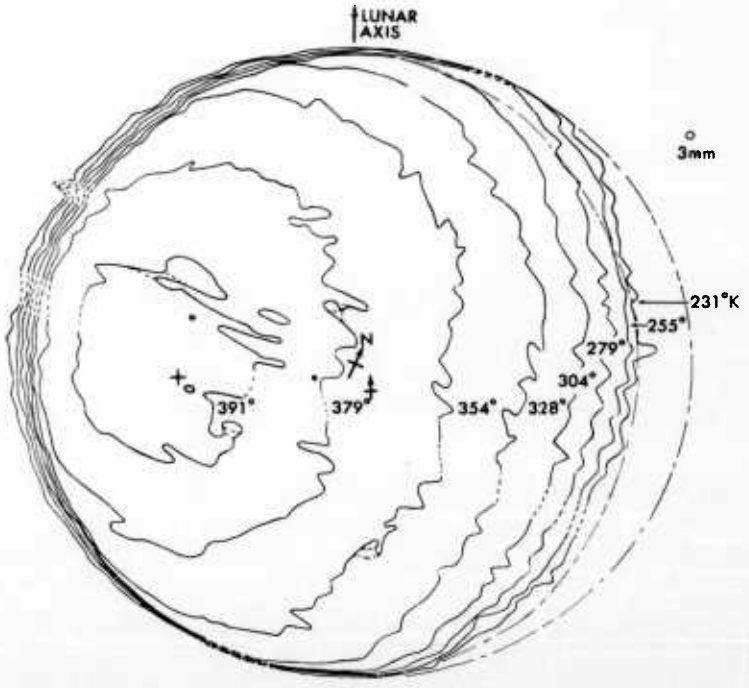

Fig. 8 Isothermal Contours of January 27, 1959, Start 7:42, End 10:39 Ut, 60 Scans, 0.92 Illuminated (—18 Day Old Moon)

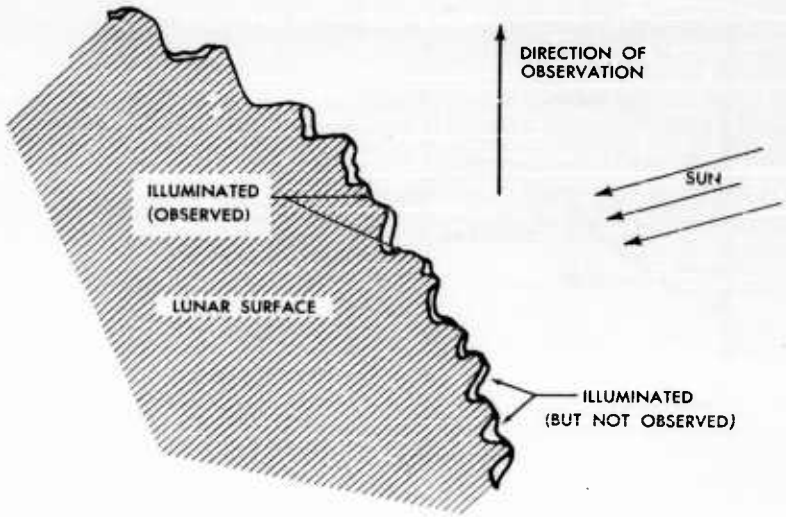

Fig. 9 Roughness Factor Explanation of Decrease in Observed Subsolar Energy for Phase Angles Other Than at Full Moon

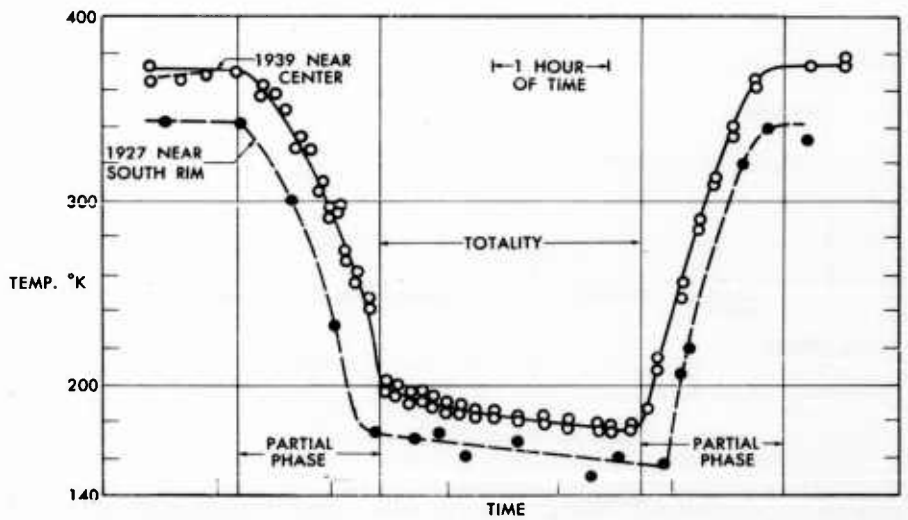

Fig. 10 Eclipse Cooling Curves for One Point 1927 and 1939 After Pettit and Nicholson

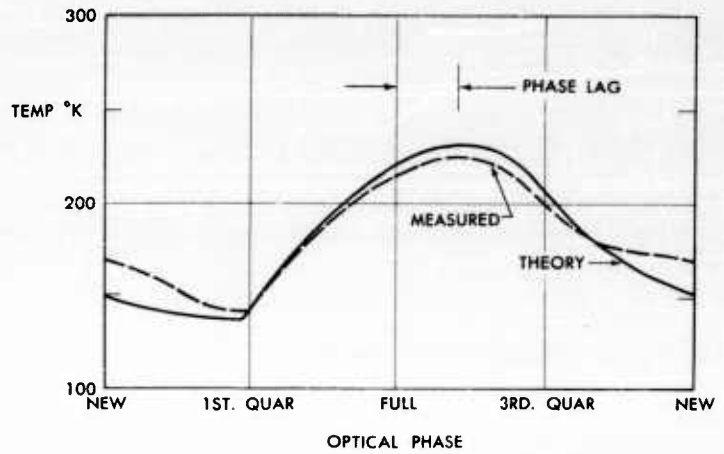

Fig. 11 Result of Gibson's Radio Measurements at 8.6 mm for Center of Lunar Disk

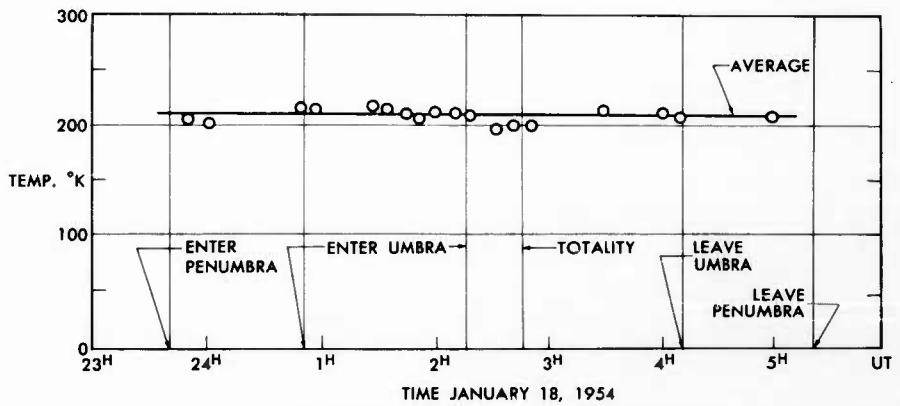

Fig. 12 Gibson's Observed Temperatures During Total Eclipse at 8.6 mm (Altitude 17° at Start)

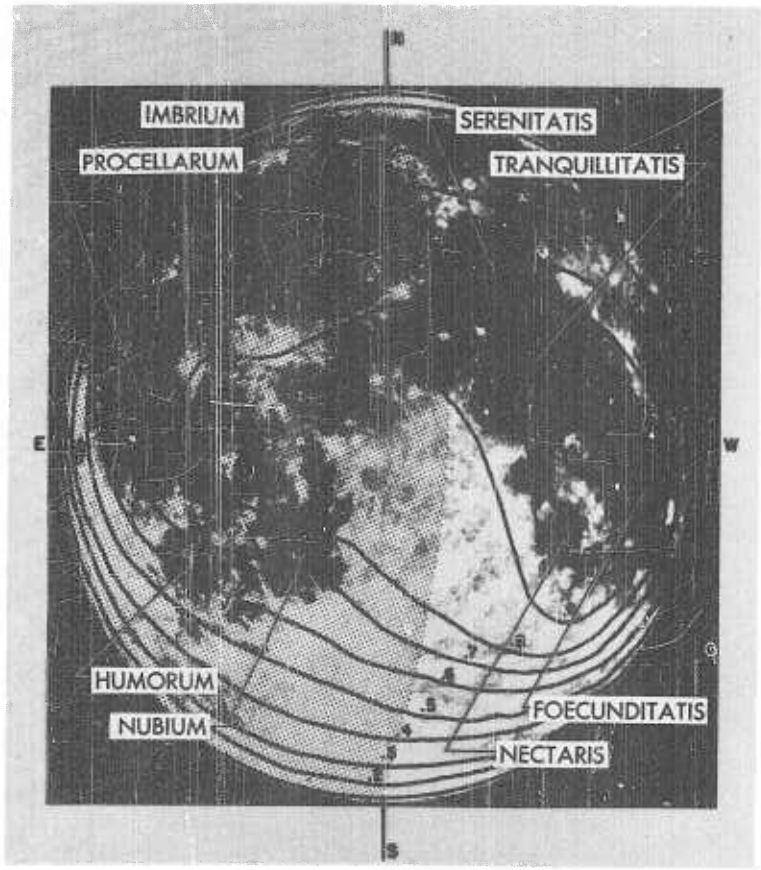

Fig. 13 Brightness Contours at 4.3 mm
Wavelength 77° Lunar Phase

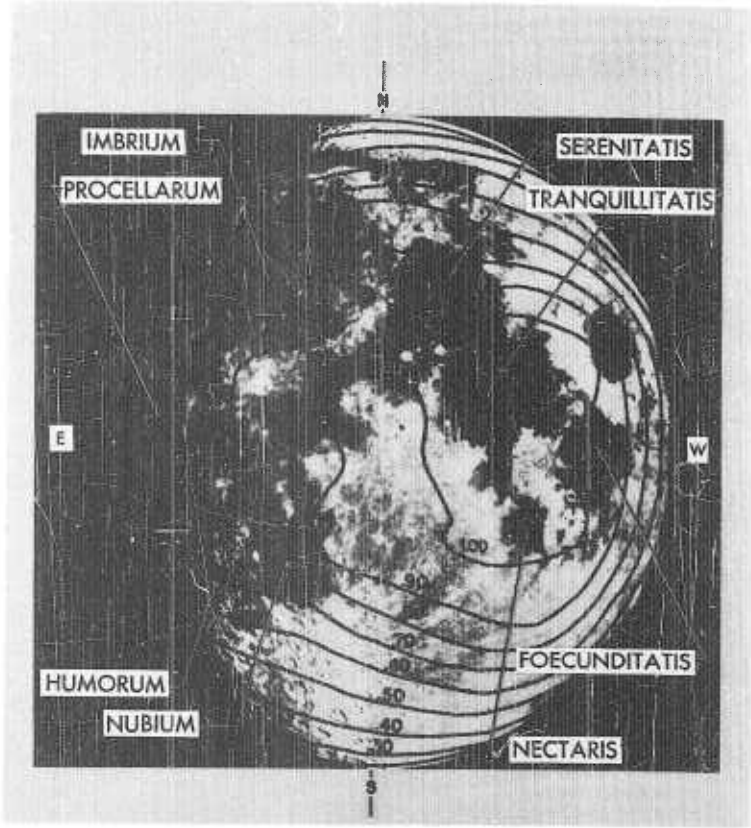

Fig. 14 Brightness Contours at 4.3 mm
Wavelength 126° Lunar Phase

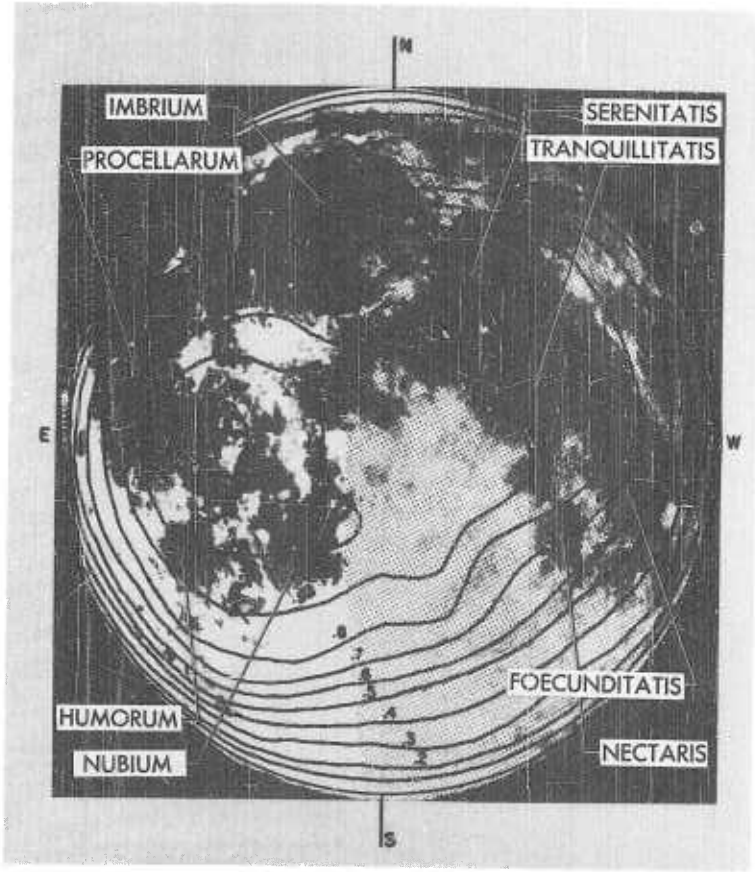

Fig. 15 Brightness Contours at 4.3 mm Wavelength 280° Lunar Phase

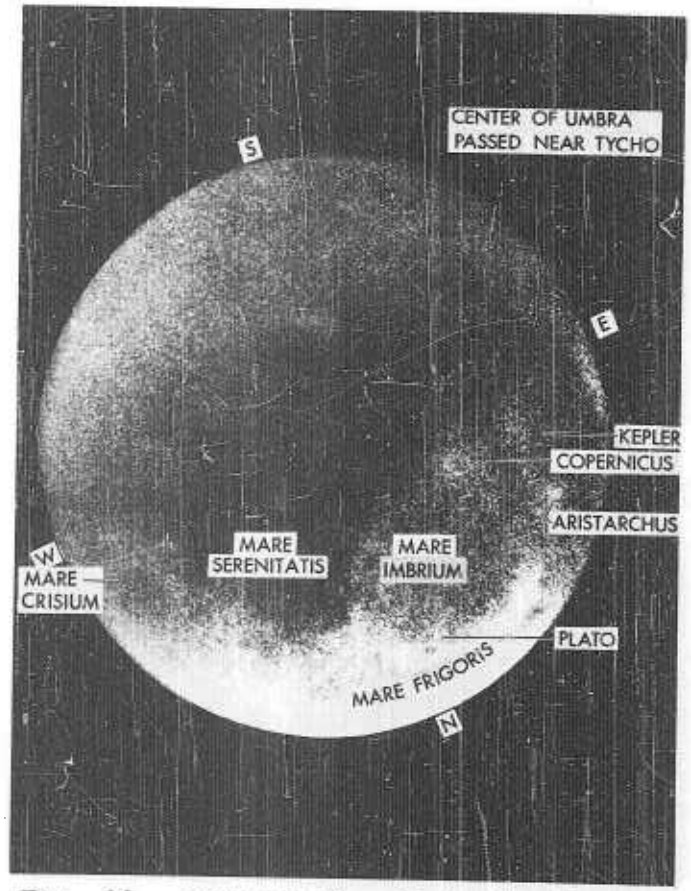

Fig. 16 Eclipsed Moon September 5, 1960 (During Totality)

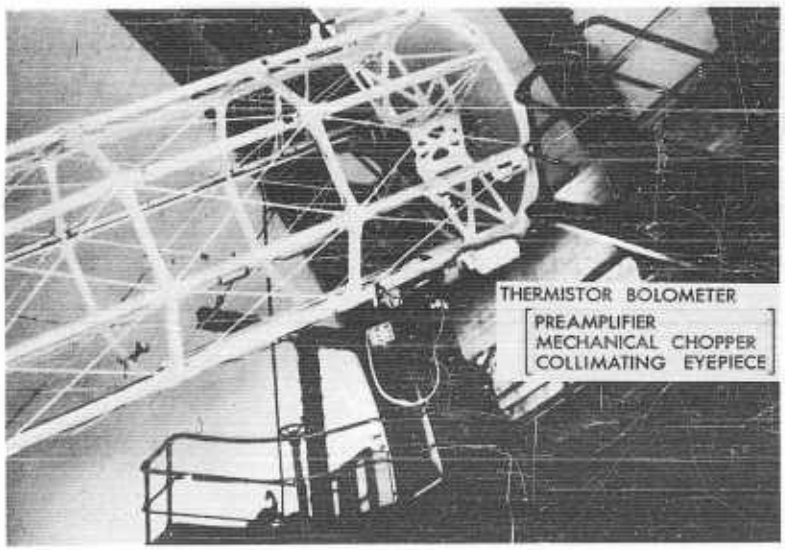

Fig. 17 The 73-Inch Reflecting Telescope of the Dominion Astrophysical Observatory, Victoria B. C. The Detector Subtended 7'' of Arc at the f/5 Newtonian Focus

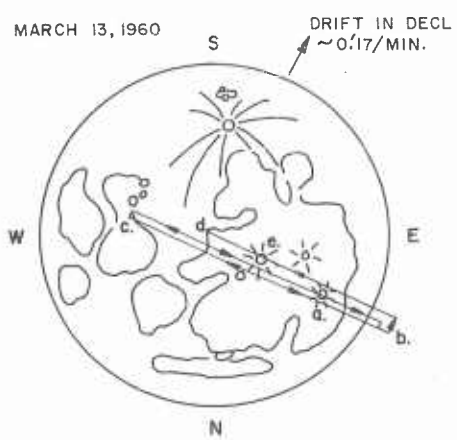

Fig. 18 Scanning Cycle March 12, 1960 a. Aristarchus b. End of Scan Off East Limb c. End of Scan Near the Sea of Nectar d. Center of Disk, End of 14.5 Min. Scan Cycle e. Copernicus

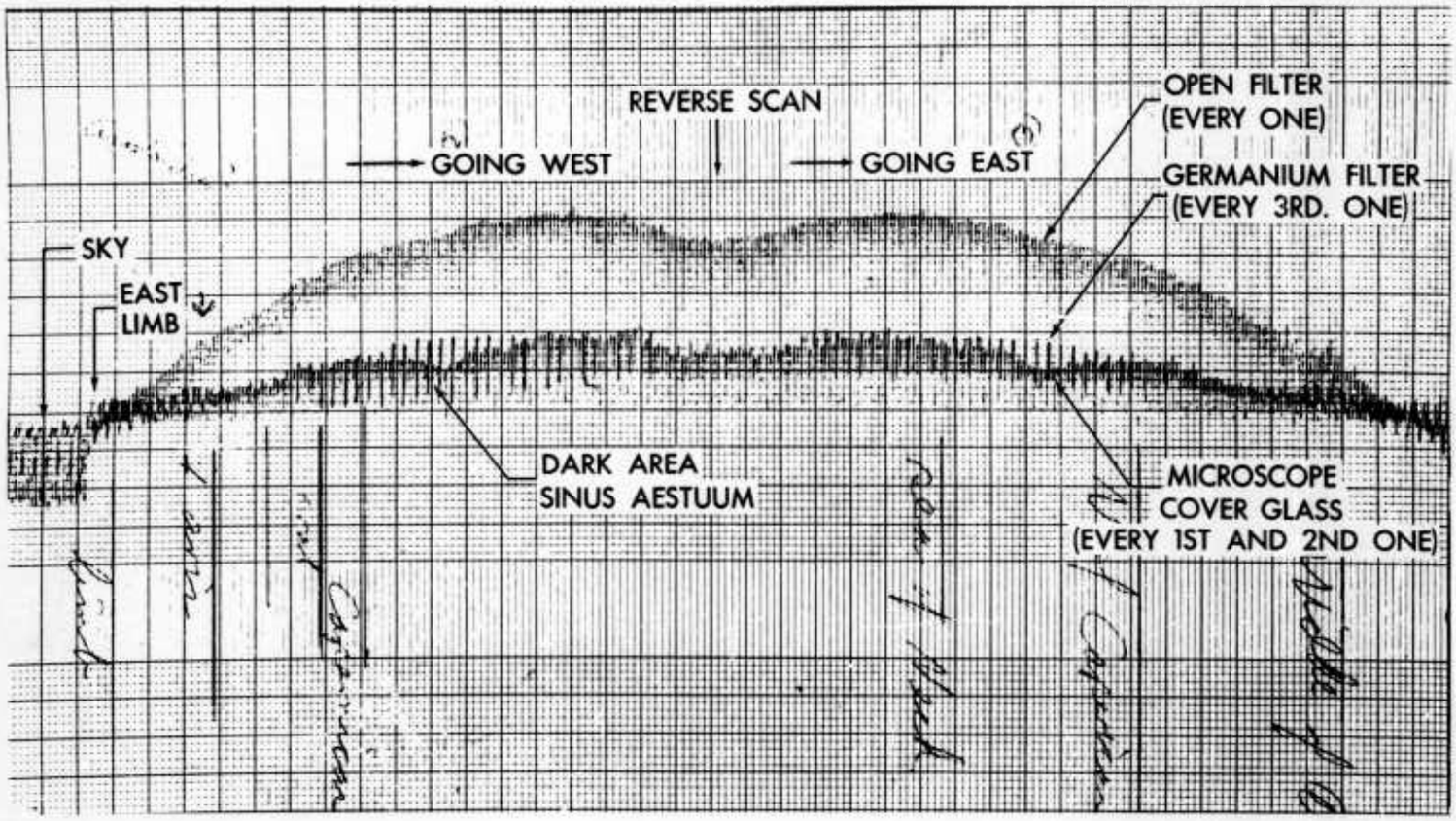

Fig. 19 Scan Over the Lunar Surface with Rotating Filter Wheel During the Full Moon March 12, 1960 (The Open Filter Shows Radiation 0.5 to 15 Microns. The Microscope Cover Glass Shows the Radiation 0.5 to 5 Microns. The Germanium Filter Shows the Radiation 2 to 15 Microns.)

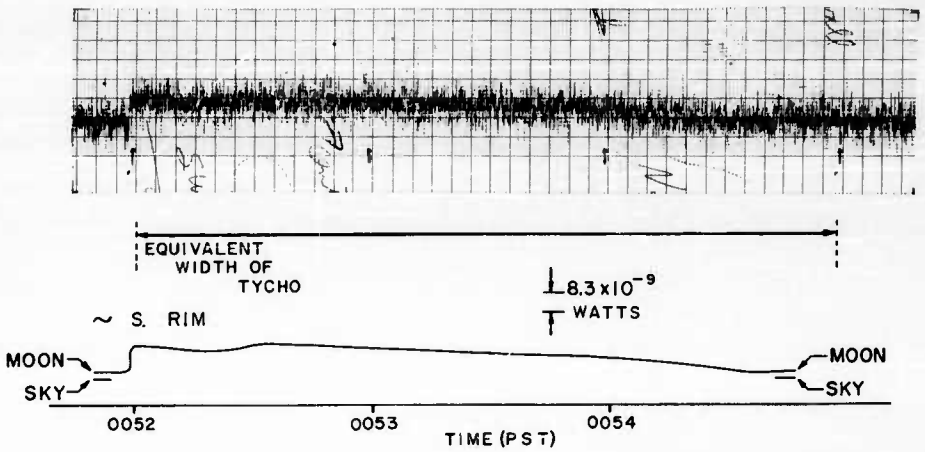

Fig. 20 Original and Smoothed Data from a Typical Scan of the Crater Tycho March 12, 1960

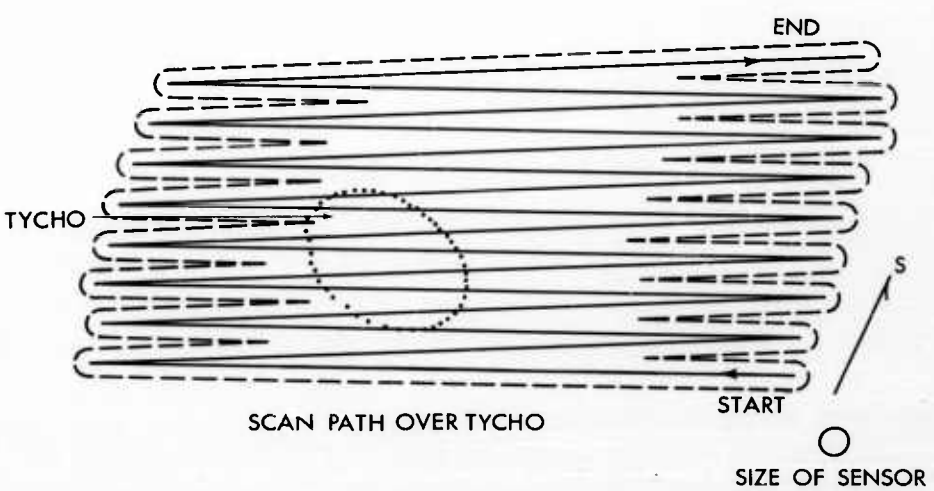

Fig. 21 Scan Path Over Tycho September 5, 1960

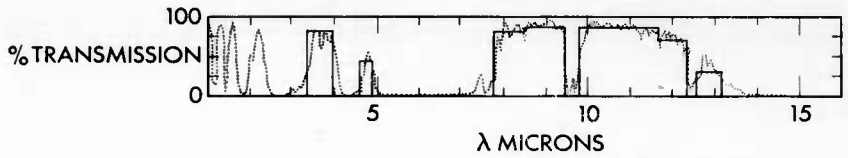

Fig. 22 Simulated Atmospheric Transmission Curve

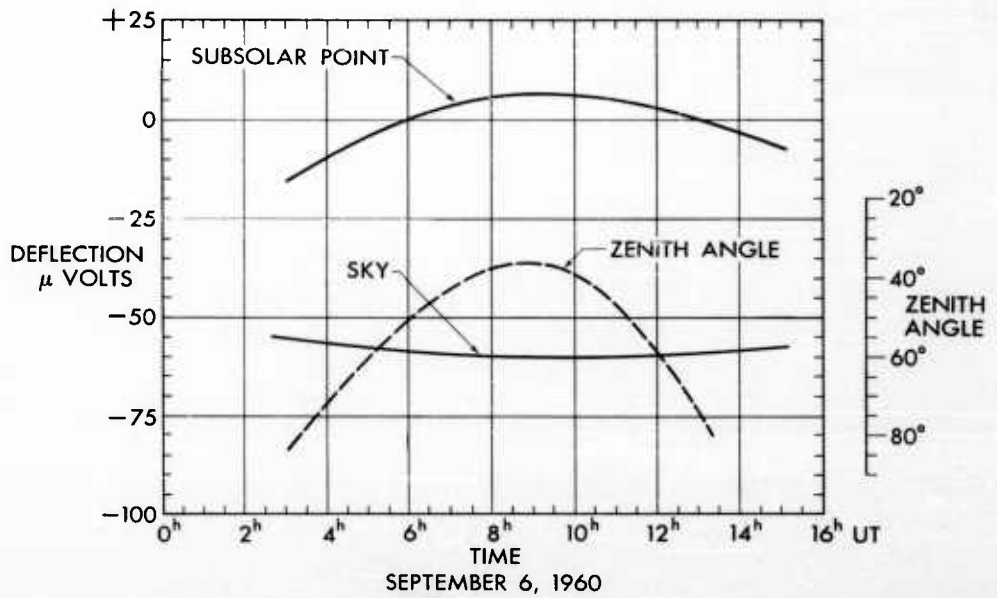

Fig. 23 Calibration Curves From Sky and Subsolar Point Readings

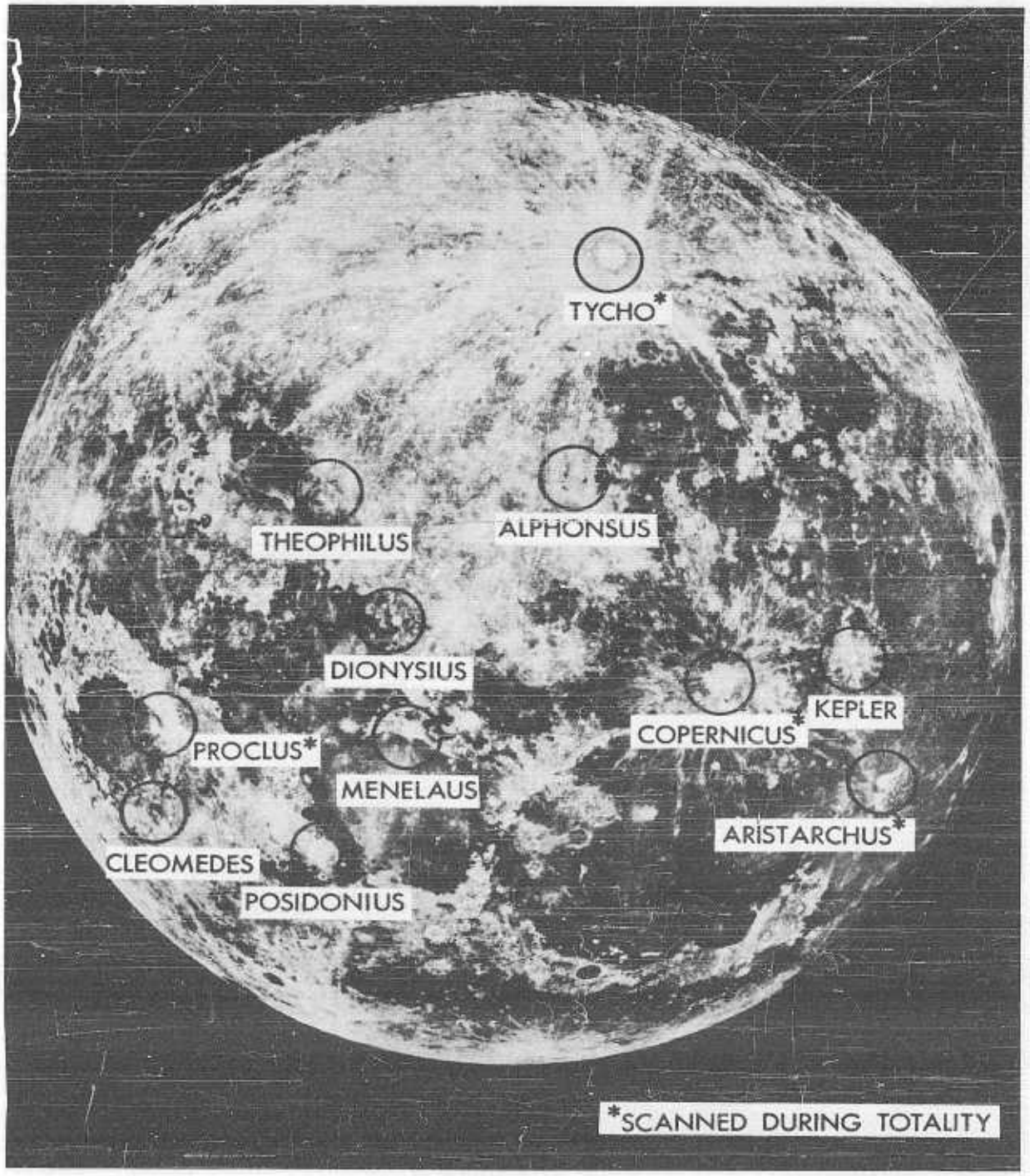

Fig. 24 Crater Region Scanned, September 4, 5, 6 1960

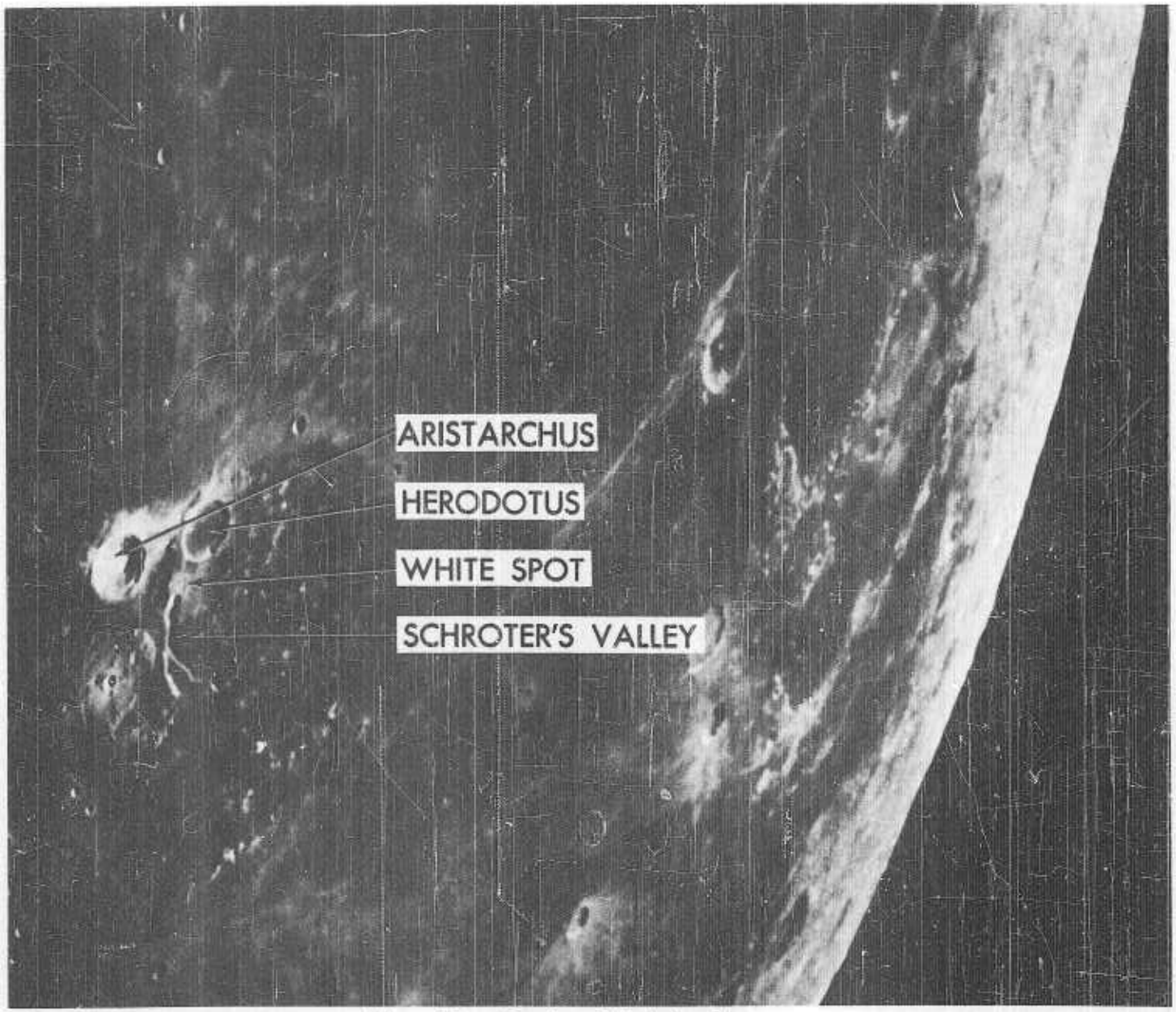

Fig. 25 Region of Aristarchus

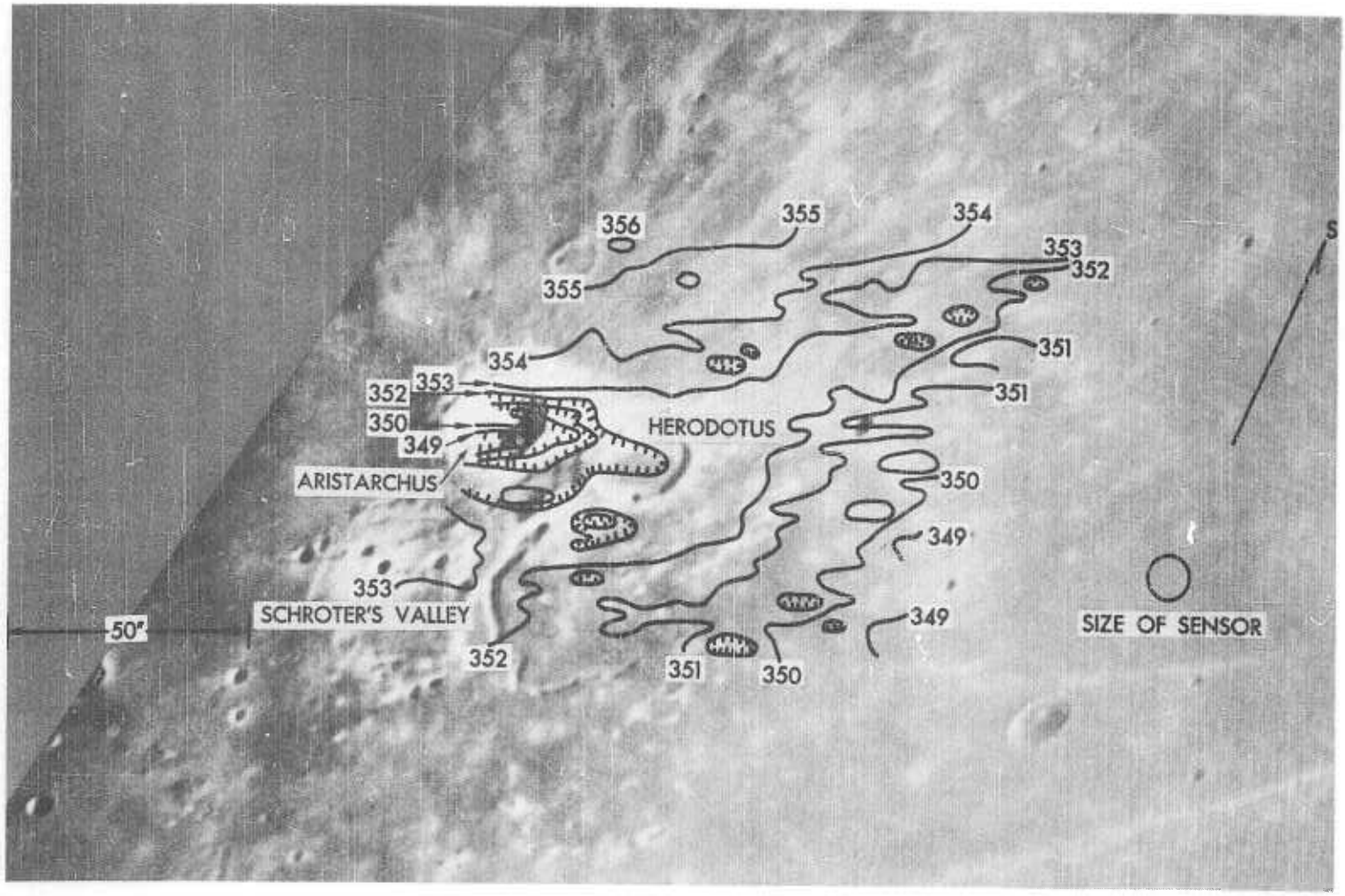

Fig. 26 Isotherms in the Region of Aristarchus September 6, 1960, 6:56 UT

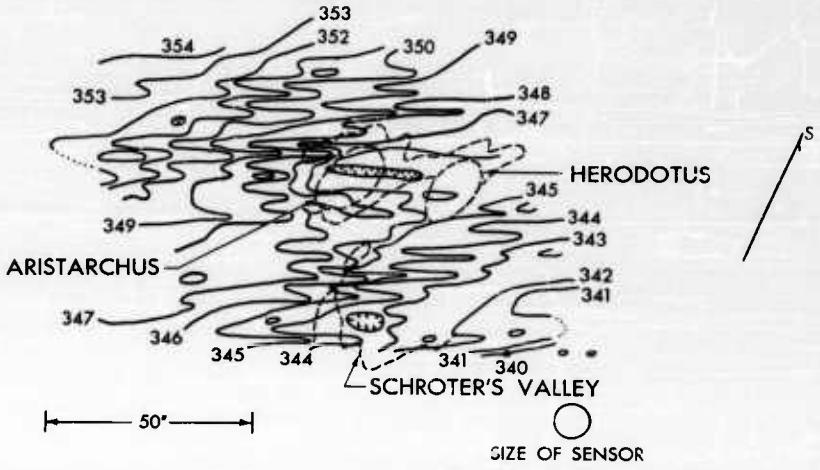

Fig. 27 Isotherms in the Region of Aristarchus
September 5, 1960, 6:57 UT

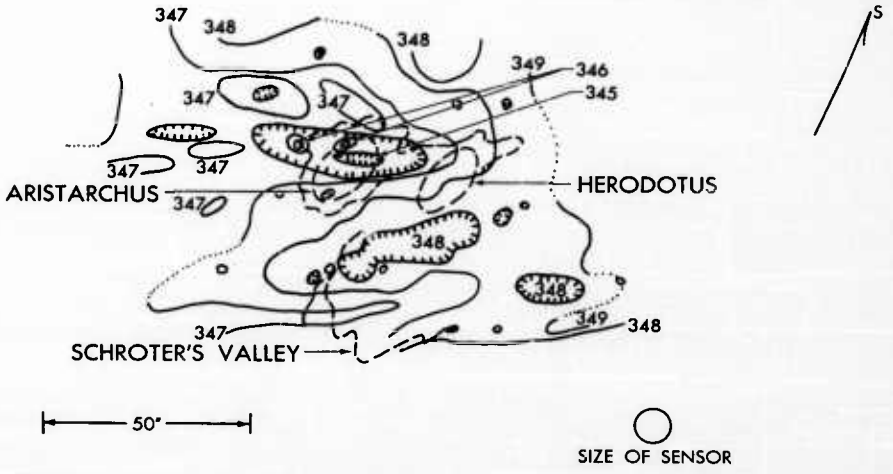

Fig. 28 Isotherms in the Region of Aristarchus Rectified to Remove the Effect of the Curvature of the Surface
September 5, 1960, 6:57 UT

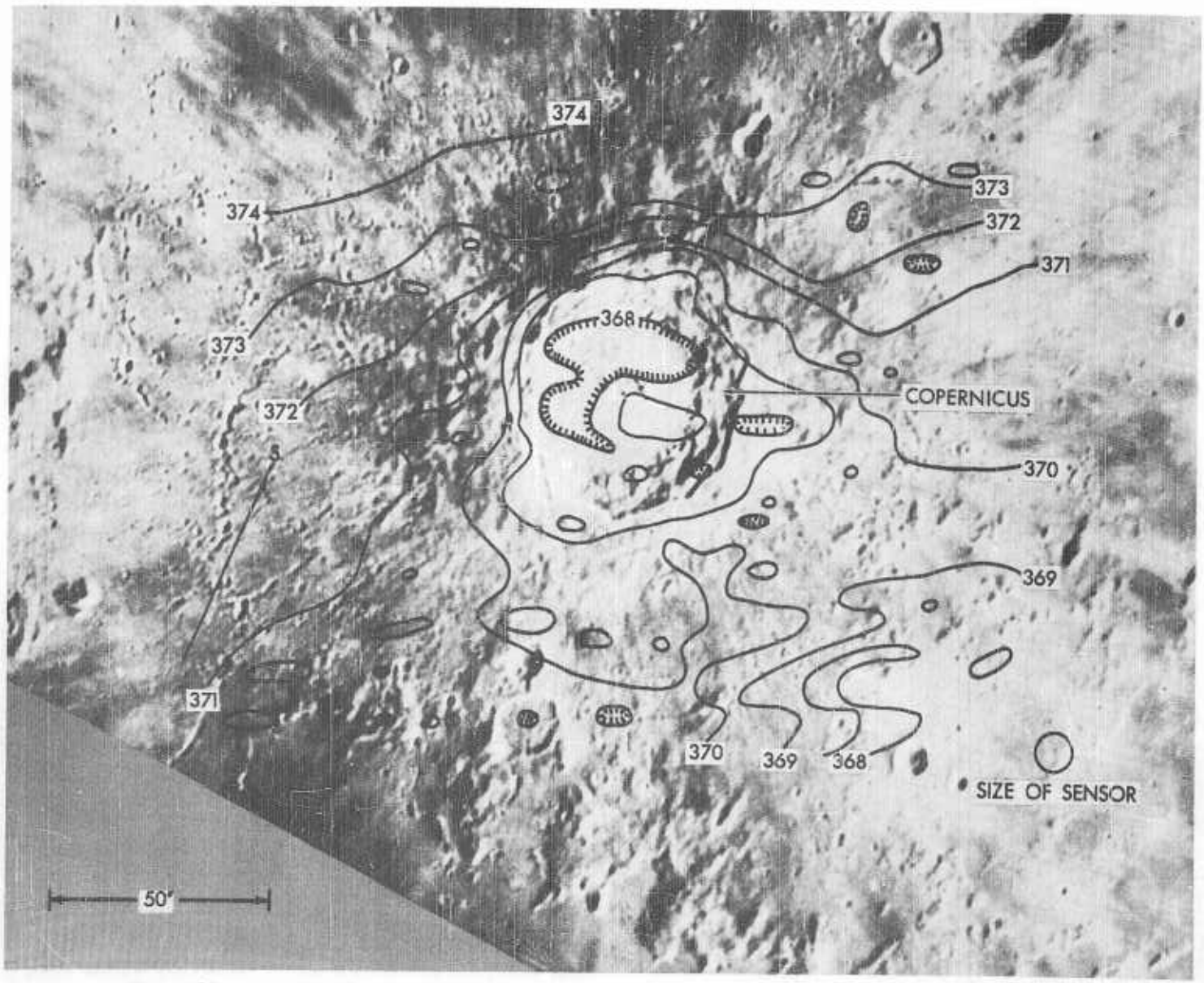

Fig. 29 Isotherms in the Region of Copernicus September 6, 1960, 6:27 UT

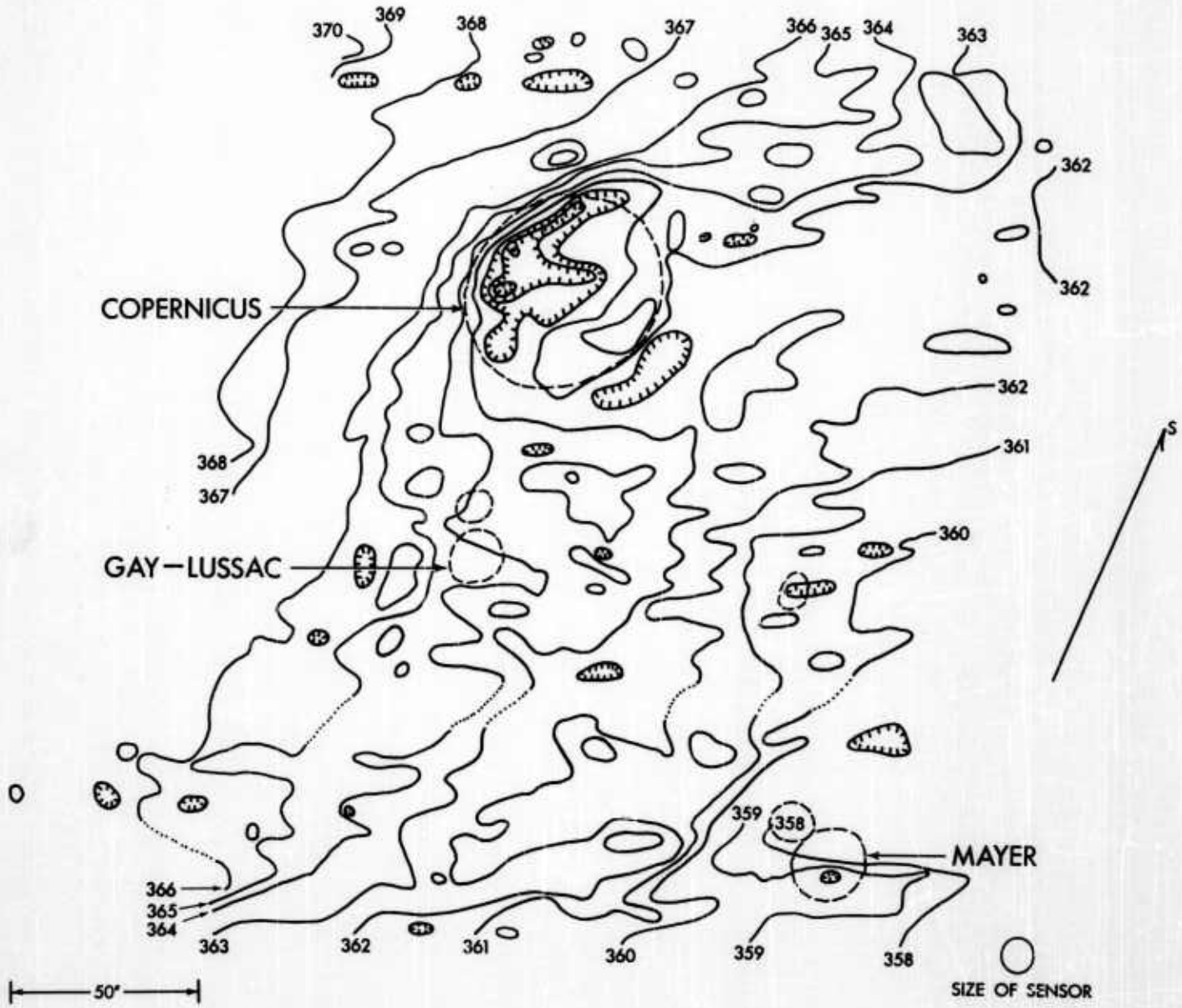

Fig. 30 Isotherms in the Region of Copernicus Setember 5, 1960, 5:48 UT

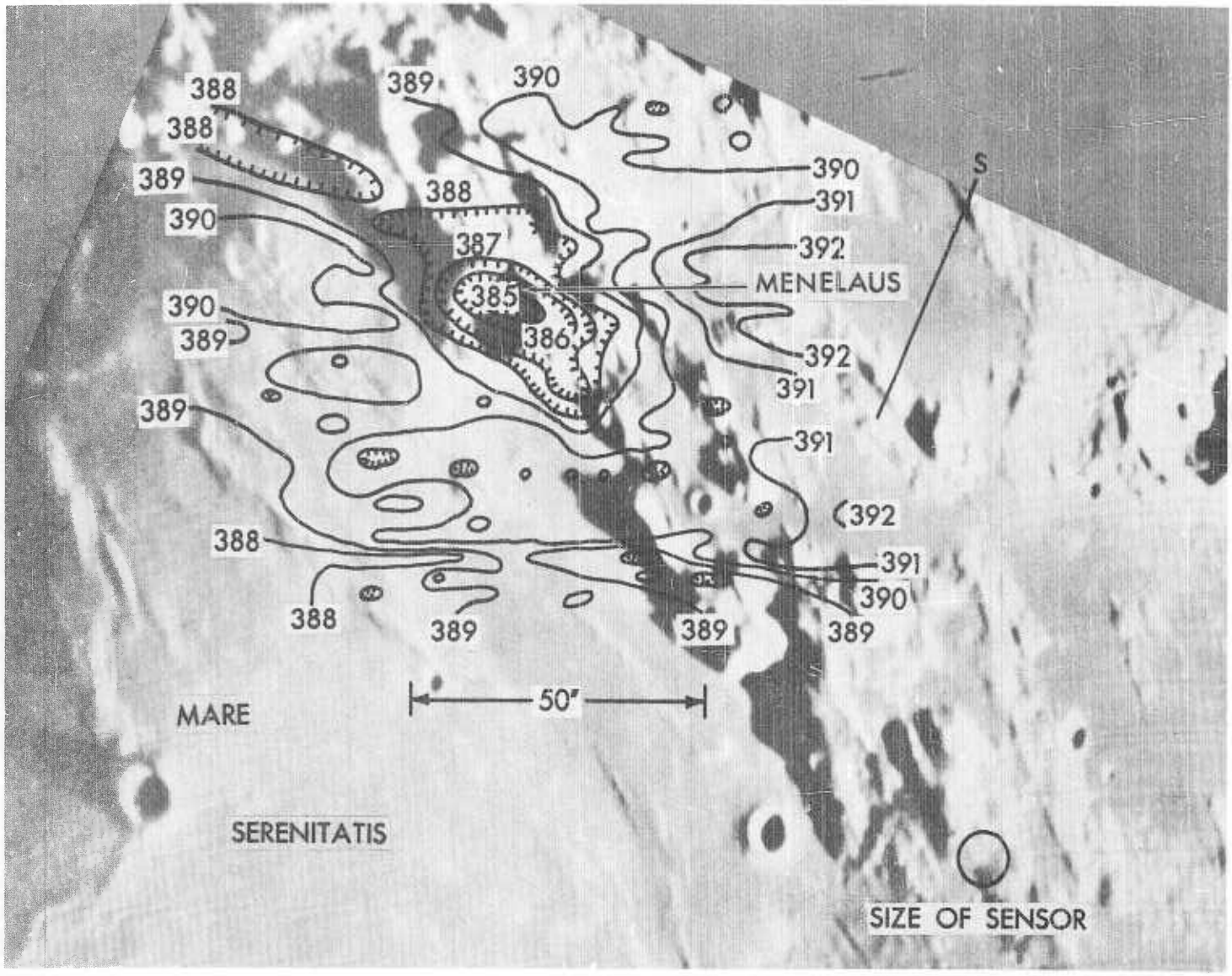

Fig. 31 Isotherms in the Region of Menelaus September 5, 1960, 7:44 UT

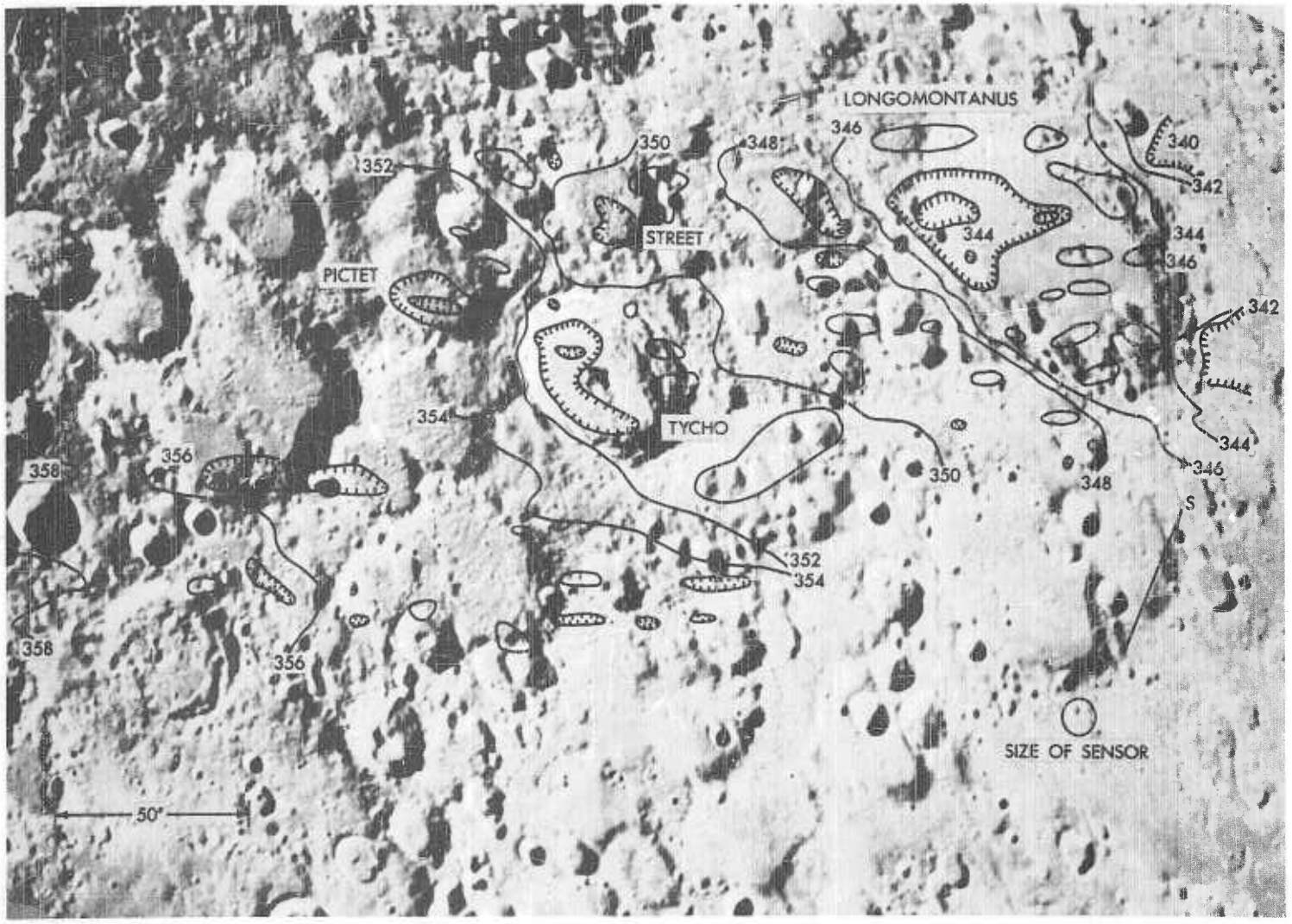

Fig. 32 Isotherms in the Region of Tycho September 5, 1960, 5:18 UT

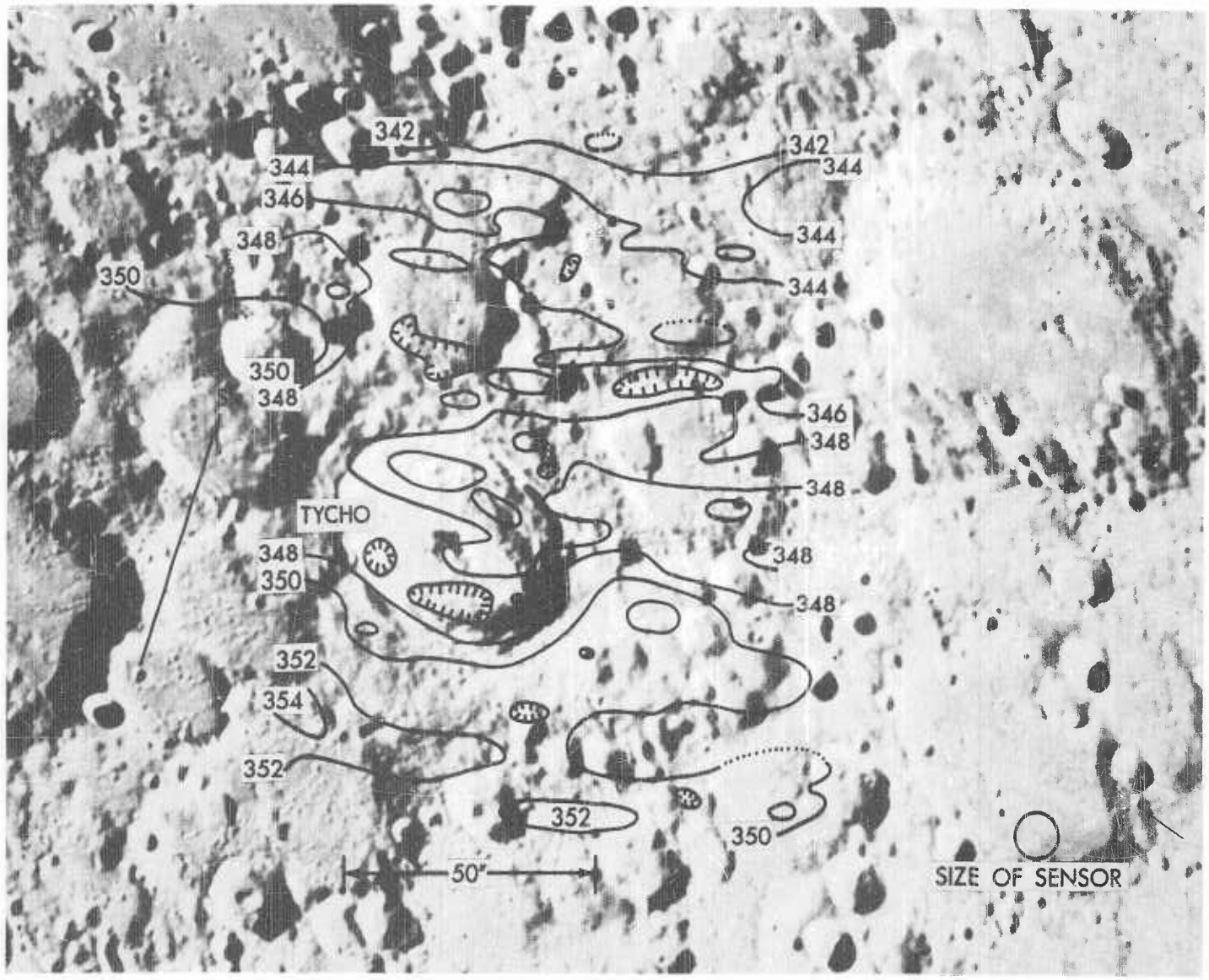

Fig. 33 Isotherms in the Region of Tycho September 6, 1960, 5:50 UT

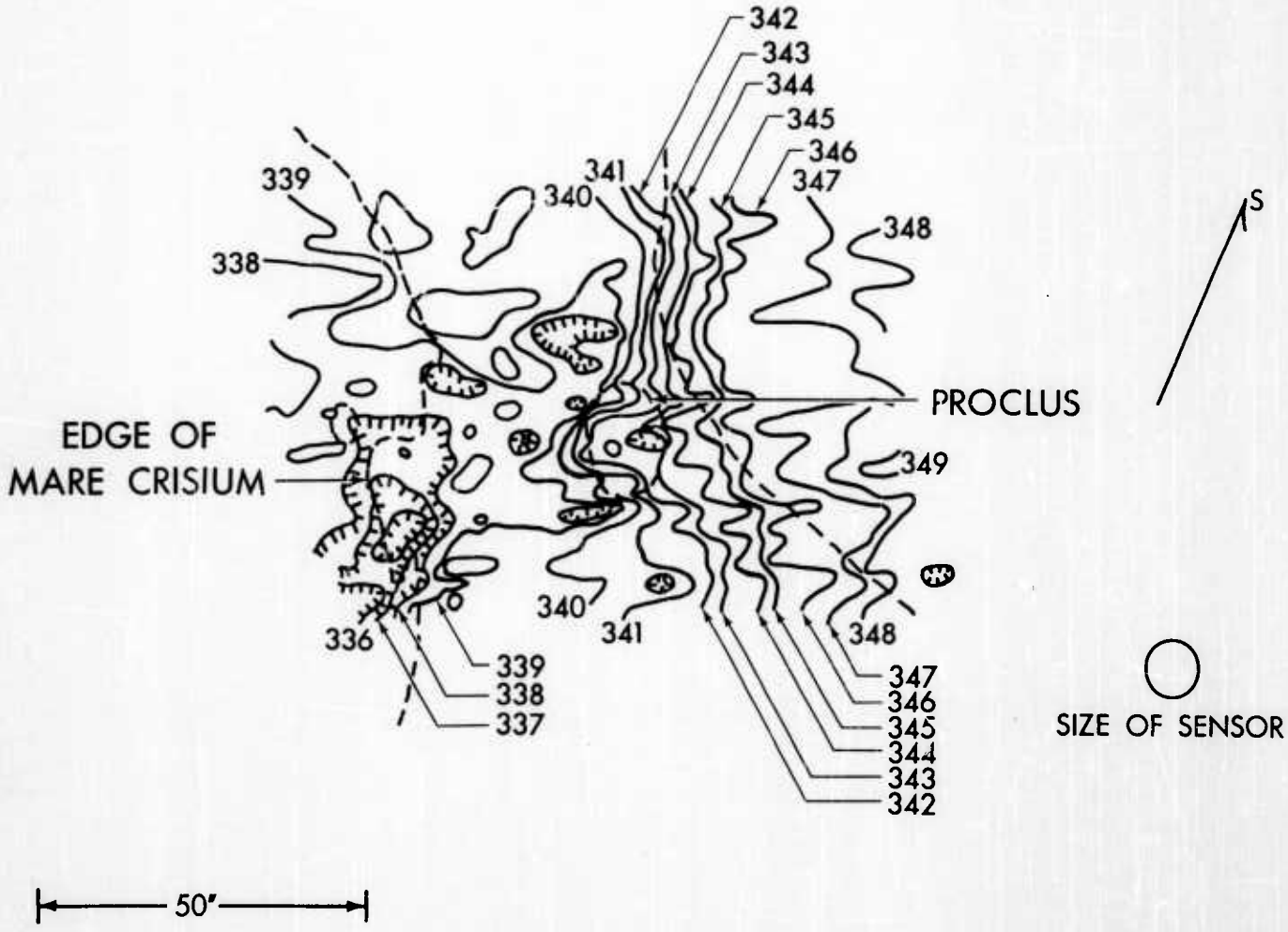

Fig. 34 Isotherms in the Region of Proclus September 6, 1960, 7:54 UT

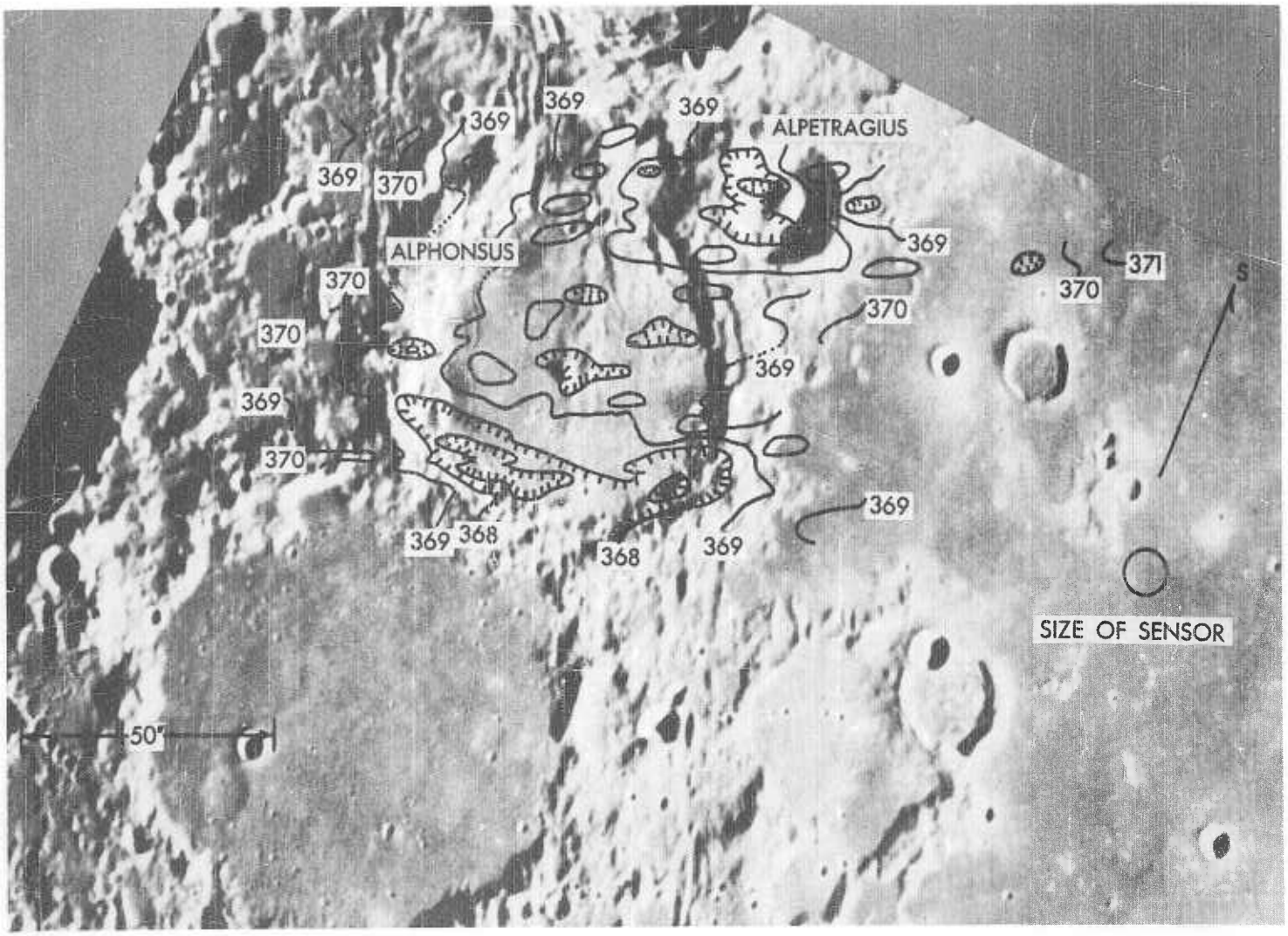

Fig. 35 Isotherms in the Region of Alphonsus September 5, 1960, 6:18 UT

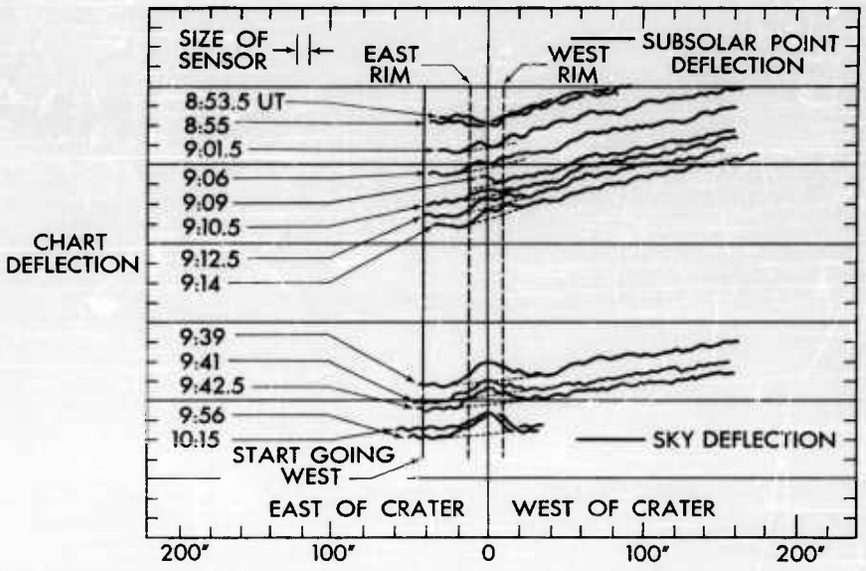

Fig. 36 Temperature Traces Over Aristarchus During Eclipse, September 5, 1960

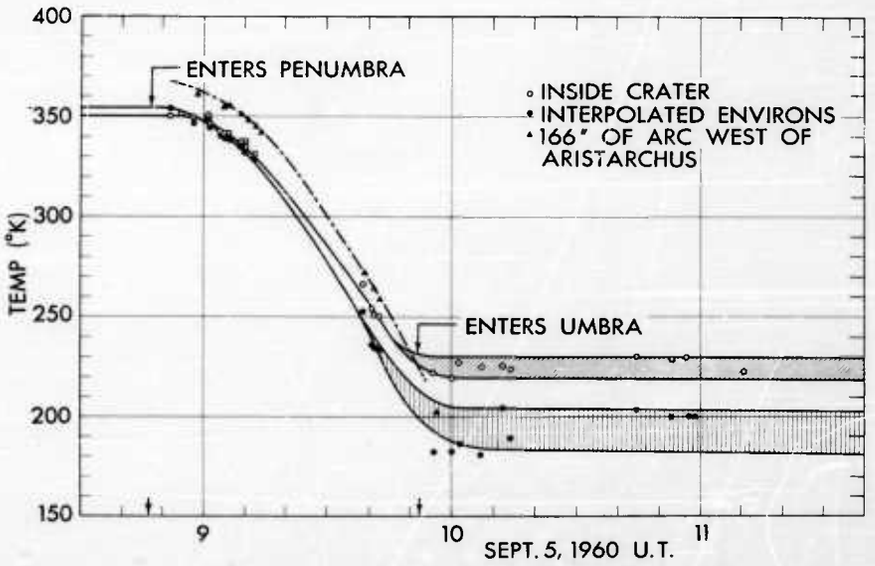

Fig. 37 Eclipse Cooling Curve for the Crater Aristarchus and its Environs

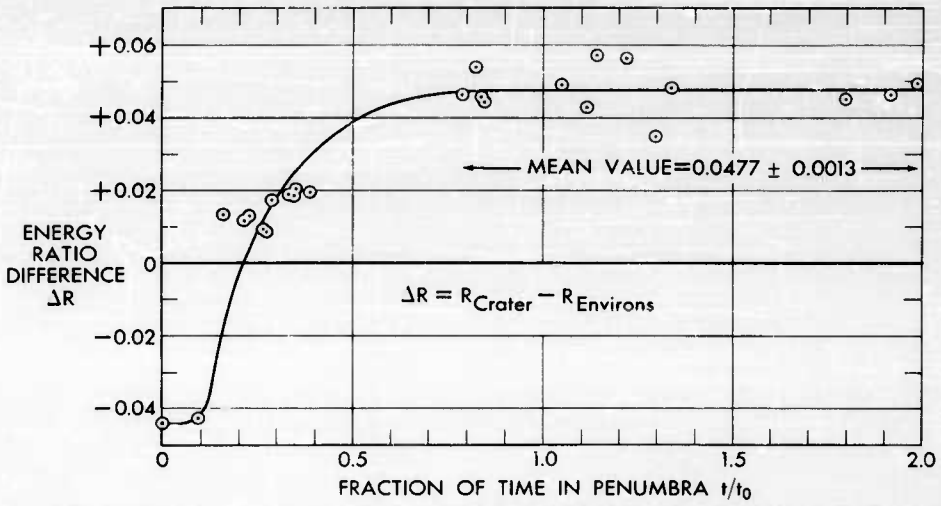

Fig. 38 Difference in Energy Ratios Between Crater and Interpolated Environs for Aristarchus September 5, 1960, Eclipse

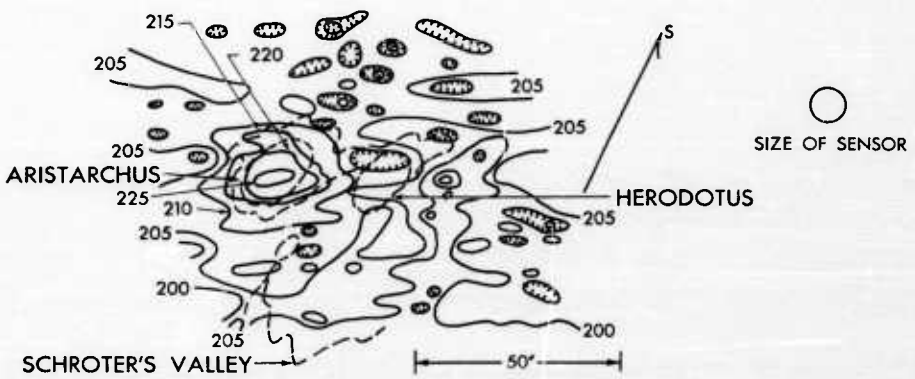

Fig. 39 Isotherms in the Region of Aristarchus During Eclipse September 5, 1960, 10:12 UT

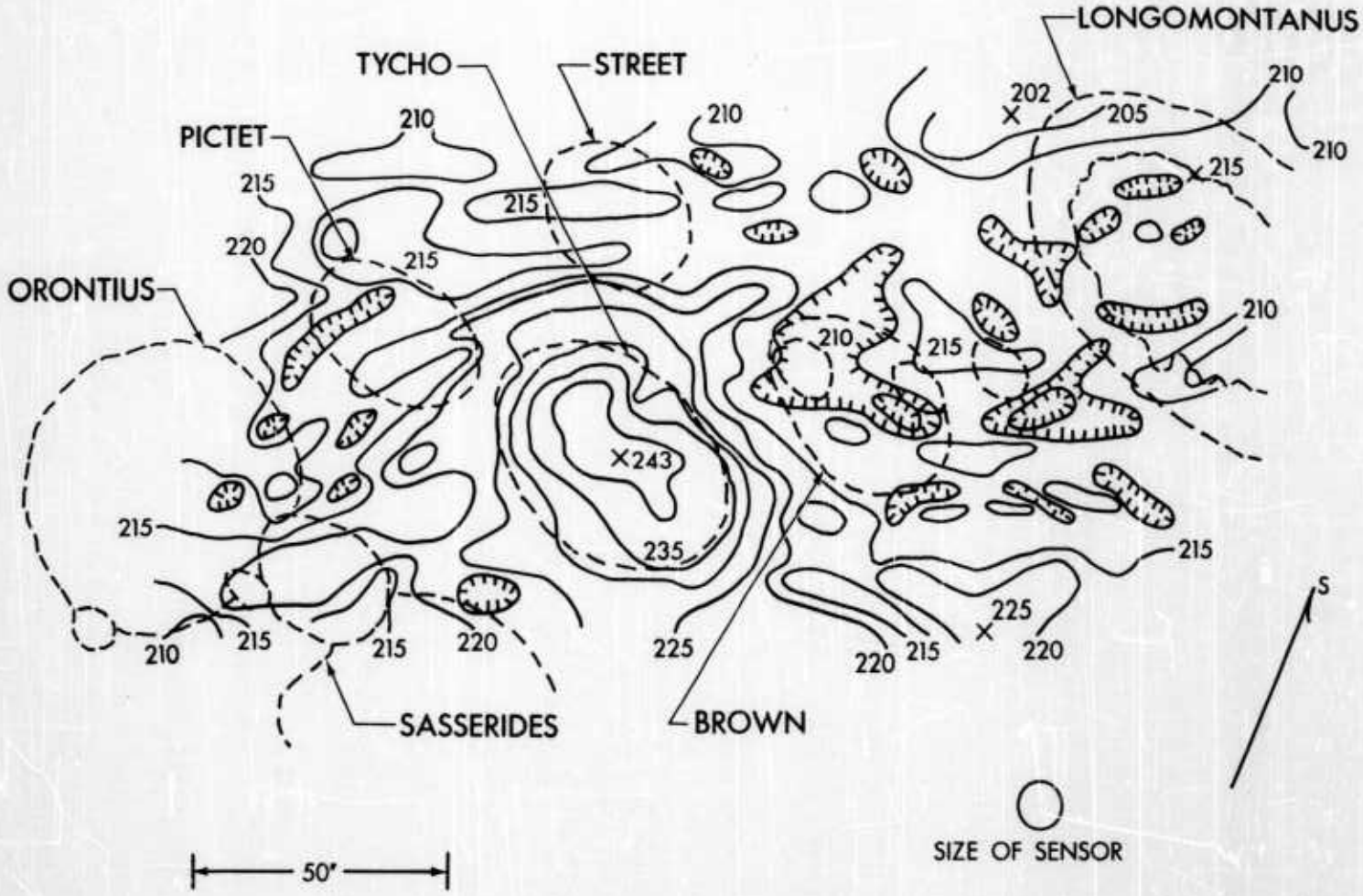

Fig. 40 Isotherms in the Region of Tycho During Eclipse September 5, 1960, 10:34 UT

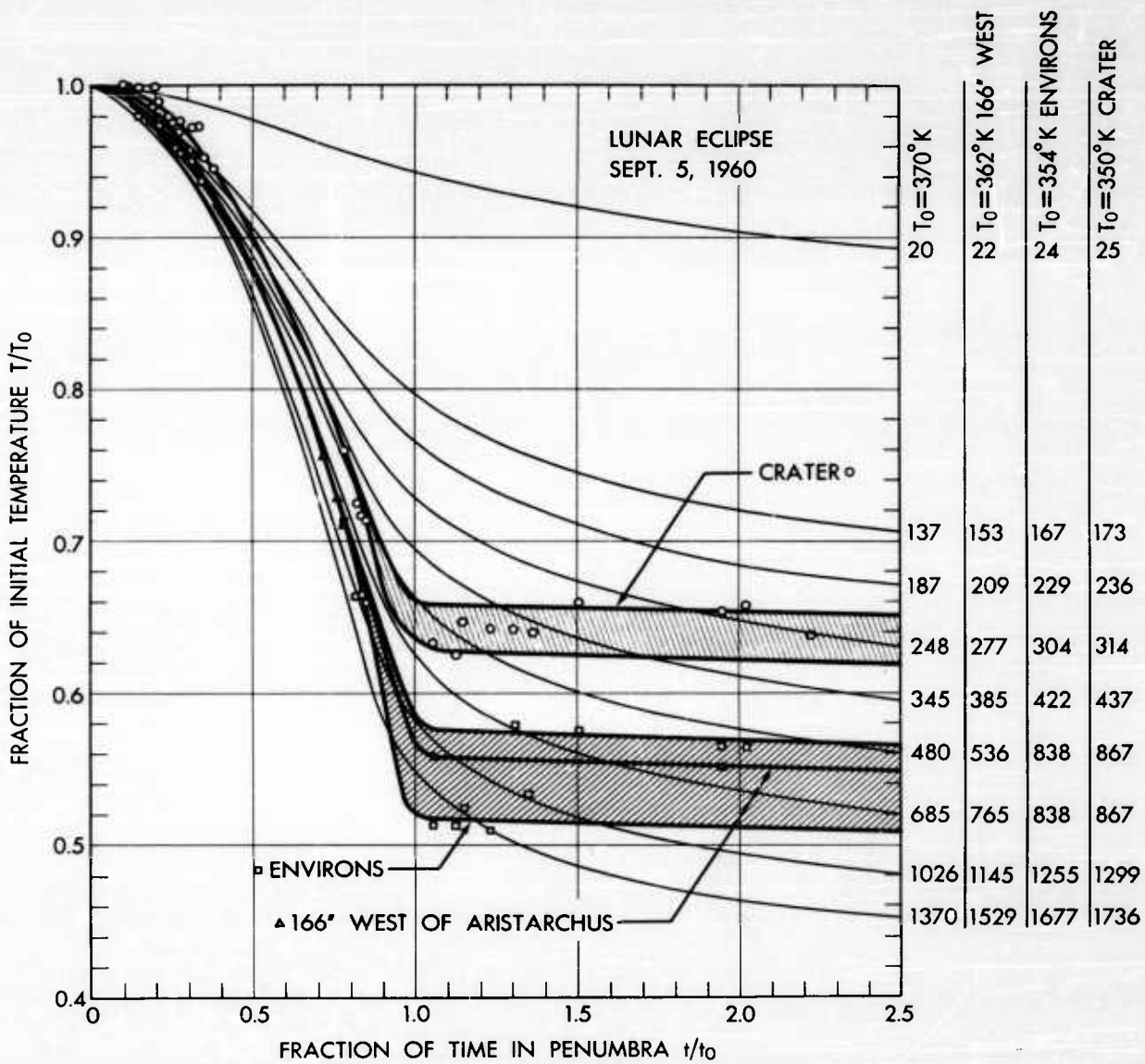

Fig. 41 **Normalized Cooling Curves for Aristarchus and its Environs; Experimental Values and Theoretical Homogeneous Surface with Different $(K\rho c)^{-1/2}$ Values**

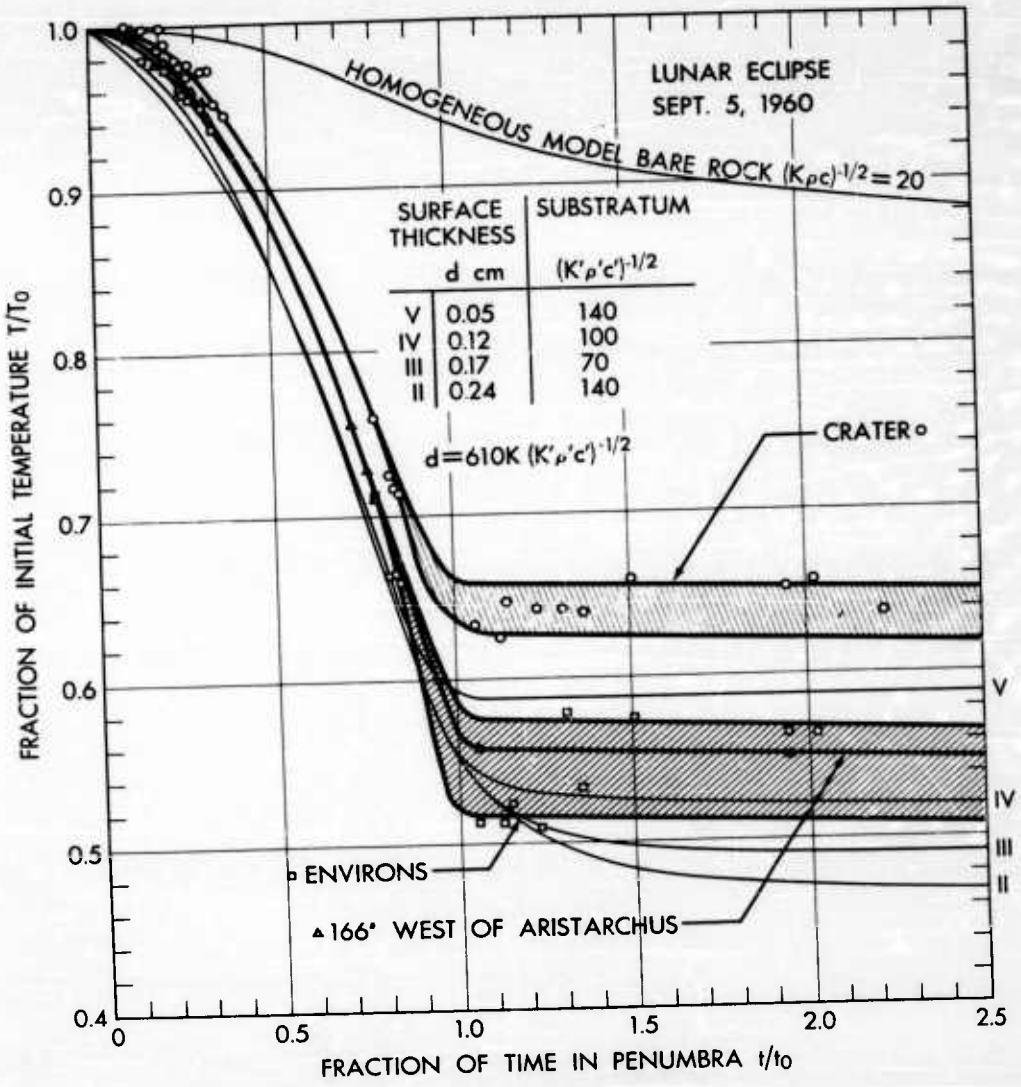

Fig. 42 **Normalized Cooling Curves for Aristarchus and its Environs; Experimental Values and Theoretical Two-Layer Model**

UNCLASSIFIED